FINAL REPORT:

RESPONSE OF JOINT DOMINATED SPACE STRUCTURES

CARNEGIE INSTITUTE OF TECHNOLOGY

CARNEGIE MELLON UNIVERSITY

AUGUST 1987

1. Introductory Comments

This document reports the work completed on the NASA research grant NAG-1-612, entitled "Response of Joint-Dominated Space Structures." The work falls into two categories: 1) developing an efficient method for calculating the transient response of a nonlinear system such as a large joint-dominated space structure and 2) investigating the effect of gravitational loading and joint scaling on the dynamic response of model structures. The results of the investigations on these two topics are reported in Section 2 and Section 3, respectively.

2. Transient Response of Joint Dominated Space Structures: A New Linearization Technique

G. A. Foelsche
J. H. Griffin
J. Bielak

Carnegie Institute of Technology
Carnegie Mellon University
Pittsburgh, PA 15213

Transient Response of Joint Dominated Space Structures: A New Linearization Technique

by

G. A. Foelsche, J. H. Griffin, and J. Bielak
Carnegie Mellon University
Pittsburgh, Pennsylvania 15213

Abstract

A new, efficient linearization method is presented for calculating the transient response of nonlinear systems due to initial disturbances. The method is an extension of the describing function approach in which the steady-state response of the system is calculated by representing the nonlinear element, typically joints in the the case of space structures, by impedances which are functions of the amplitude of response. Thus, the problem of solving the differential equation for the steady-state response becomes one of solving a set of nonlinear algebraic equations involving the steady-state amplitudes and phases of the system. It is shown that for the transient case the steady-state impedances can be averaged over the range of response in order to provide equivalent values of stiffness and damping that, for a given set of initial displacements, may be treated as being constant for purposes of calculating system response.

Single-degree-of-freedom systems are used first to demonstrate the method and then to develop an approach for optimizing the joint's characteristics so as to minimize transient response times. The use of this method for response estimation and optimization in multiple-degree-of-freedom systems is investigated subsequently.

Nomenclature

B	amplitude of x (slowly varying with time)
c, c_1, C	viscous damping
c_{eff}	effective value of instantaneous system damping
f_n	force from nonlinear friction element
F_c, F_s	fundamental Fourier coefficients of f_n

k, k_i, $\mathbf{K}$, $\mathbf{K}_q$	stiffness
k_d	stiffness of nonlinear friction element
k_{eff}	effective value of instantaneous system stiffness
m, m_i, $\mathbf{M}$	mass
N	normal load on friction contact
t	time
Δt	half period
$\mathbf{u}_i$	eigenvectors
x, $\mathbf{x}$, x_i	displacements
y, y_i	modal displacements

Greek

γ_i	eigenvalues of linearized system
μ	coefficient of friction
ϕ	phase lag
θ	$\omega t - \phi$
θ^*	θ value at which nonlinear element transitions from stick to slip
ω	frequency
ω_d, ω_n	natural frequencies
ζ	fraction of critical damping

Superscripts

*	nondimensionalized quantities
(-)	quantities averaged over a range of response

Additional

Bold type indicates a vector or matrix quantity

Introduction

An important problem related to the design of space structures is that of predicting their dynamic response. This process is particularly difficult when dealing with structures that contain a large number of joints that exhibit nonlinear, hysteretic behavior. For example, this may be the case for prefabricated truss structures that are designed to collapse into a dense package for transportation to orbit. The truss is then expanded in space by utilizing joints that are especially designed to rotate and lock into place. The dynamic response of such structures is said to be joint dominated if the amount of damping or the stiffness of the system is strongly affected by the joints' behavior. If damping in the system is primarily due to joint hysteresis then joint behavior controls the amplitude of the steady state response as well as the rate at which transients decay. Additionally, in some cases, joint flexibility can significantly reduce the stiffness of the structure, thus reducing its natural frequencies and altering the associated mode shapes. This paper discusses a new approach that may be used to efficiently estimate the transient response of such systems.

The transient response of nonlinear systems is usually calculated by time integration methods that employ finite differences in time; see, for example, Hughes [1]. This approach has two disadvantages when it is applied to the design of joint dominated structures. The first is that it is computationally intensive. This would be especially the case for the type of complex three-dimensional truss structures that are proposed for space applications since they have a large number degrees of freedom. Secondly, the problem is nonlinear and, consequently, the solutions lack generality. For example, the rate of decay of a transient would depend on the specific magnitude and distribution of the assumed initial displacements and velocities of the structure. Since the number of degrees of freedom is large, it is not reasonable to consider all possible initial conditions. So one difficulty faced by the design engineer is in trying to select those conditions that are of critical importance to the design and to simulate the corresponding system response when there is such a large number of possible cases to consider. Neither the selection nor the simulation process is particularly feasible if time integration is the only procedure available for calculating the response of the system.

In this paper an approximate method is developed for estimating the transient response of nonlinear systems in terms of linearized modes of response. Its advantages are that it is computationally more efficient than the time integration

method and that it is possible to view the design problem in the more traditional physical terms of modal response. For example, if it is most important to damp the larger amplitude, low frequency response one can easily focus on that issue by isolating the response of the first few linearized modes. Consequently, by utilizing this approach the design problem should become more tractable. The major drawback of the approximate method is loss of accuracy. It is our view that both approximate methods and time integration have their roles in design. Approximate methods provide efficient tools for performing parametric studies and they supply physical insights into how to optimize system performance that are not easily inferred from strictly numerical methods. Time integration provides a method for assessing the accuracy of the approximate solution for key simulations and for fine tuning the final design.

In the procedure presented here the nonlinear system is approximated by an equivalent linear system in which the system parameters are constant over the range of transient response. The method is an extension of the describing function approach used to calculate the steady-state harmonic response of nonlinear systems. In the describing function approach the response is assumed to be essentially harmonic and the nonlinear element is represented by impedances which depend on the amplitude of response. As a result, the problem of solving the differential equation for the steady-state response becomes one of solving a set of nonlinear algebraic equations for the steady-state amplitudes and phases associated with the various degrees of freedom of the system. In the transient case considered here the steady-state impedances are averaged over the range of response in order to provide equivalent values of stiffness and damping that, for a given set of initial conditions, may be treated as constants for purposes of calculating system response. We refer to this approach as the Amplitude Averaging (AA) Method. Once equivalent parameters are identified for the system, conventional methods can be employed for analyzing the resulting linear system. Related studies have been summarized, for instance, by Iwan and Gates [2].

The AA Method is derived from an efficient time integration procedure presented by Sinha and Griffin [3] in which single time steps were used to step from one peak of the oscillation to the next. Their approach in turn, was based on the idea that the response may be approximated as a sinusoid in which the amplitude and phase vary slowly with time (see, for example, Caughey [4]).

In the first part of this paper the AA Method is illustrated by applying it to a

single-degree-of-freedom (SDF) system exhibiting the bilinear hysteretic behavior typically associated with Coulomb friction. While the method is not restricted to this type of nonlinearity this behavior was selected for analysis because it is representative of the type of severe nonlinearity that occurs in actual joints. A half cycle method similar to that used by Sinha and Griffin is presented in order to illustrate the linearization process and in order to develop "instantaneous" values of the nonlinear element's stiffness and damping. The instantaneous values of the element's parameters, which effectively characterize the joint's properties at a given amplitude of response, are then averaged over a range of amplitudes in order to calculate the constant stiffness and damping values used in the AA Method.[1] Since an equivalent, constant damping has been determined for the system it may be used to select joint characteristics (the friction slip load in this example) so as to maximize average joint damping and minimize transient response times. In the second part of the paper a general approach that may be used for multiple-degree-of-freedom (MDF) systems is given and applied to the two body problem. In each case, the accuracy of the approach is assessed by comparing results from the approximate method with those obtained using standard time integration methods.

Single Degree of Freedom Systems (SDF)

In order to demonstrate the AA Method, we develop a solution for the bilinear hysteretic SDF system depicted in Figure 1. The equation of motion for the system is

$$m\ddot{x} + c\dot{x} + kx = -f_n \tag{1}$$

where f_n is the nonlinear force from the friction element and the dots represent differentiation with respect to time. During oscillation, the friction joint remains locked until the magnitude of the spring force, $|k_d(x-y)|$, equals the friction force μN. The joint then slips with a constant resistive force of magnitude μN until the mass reaches an extremum of oscillation, at which point the joint locks up again. The magnitude of the relative displacement (x-y) required to cause slip is designated as x_{crit}, where

[1] In the example used here to demonstrate the approach, the instantaneous joint properties are calculated analytically. Actual joint properties may be calculated from laboratory tests that measure the joint's steady state hysteresis curves. See Crawley [5] for an example of steady state joint characterization.

$$x_{crit} = \frac{\mu N}{k_d} \tag{2}$$

The Half-Cycle Method

If the transient response is approximately a sinusoid that has an amplitude and phase which vary slowly with time, then over a limited time span it may be approximated as $x = B\cos\theta$, where $\theta = \omega t - \phi$. We assume that the nonlinear force f_n exhibits the same periodicity. Expressing f_n in a Fourier series, we obtain (see Menq and Griffin, [6])

$$f_n = F_c(B)\cos\theta + F_s(B)\sin\theta + \text{(higher harmonics)} \tag{3}$$

where, for the case of Coulomb friction considered;

$$F_c(B) = \frac{k_d B}{\pi}\left[\theta^*(B) - \frac{1}{2}\sin 2\theta^*(B)\right] \tag{4}$$

$$F_s(B) = -\frac{4\mu N}{\pi}\left(1 - \frac{\mu N}{k_d B}\right) \tag{5}$$

$$\theta^*(B) = \cos^{-1}\left(1 - \frac{2\mu N}{k_d B}\right) \qquad 0 \le \theta^* \le \pi \tag{6}$$

In the case of experimental joint data, the Fourier coefficients can be calculated numerically from hysteresis curves using numerical integration.

If we keep only the fundamental harmonics and truncate the expression (3) after the first terms, we can express f_n as

$$f_n = \frac{F_c(B)}{B}x + \frac{-F_s(B)}{\omega B}\dot{x} \tag{7}$$

Thus (1) becomes,

$$m\ddot{x} + \left(c - \frac{F_s}{\omega B} \right) \dot{x} + \left(k + \frac{F_c}{B} \right) x = 0 \tag{8}$$

or,

$$m\ddot{x} + c_{eff}(B)\dot{x} + k_{eff}(B)x = 0 \tag{9}$$

where c_{eff} and k_{eff} are defined in a manner consistent with (8) and because they pertain to a specific amplitude are referred to as the instantaneous damping and stiffness of the bilinear spring. Alternatively, we may write (9) as

$$\ddot{x} + 2\zeta\omega_n\dot{x} + \omega_n^2 x = 0 \tag{10}$$

where ζ and ω_n are both functions of B

$$\zeta(B) = \frac{c_{eff}(B)}{2(m\ k_{eff}(B))^{1/2}} \tag{11}$$

$$\omega_n(B) = \left(\frac{k_{eff}(B)}{m} \right)^{1/2} \tag{12}$$

The damped natural frequency of this system may be similarly defined as

$$\omega_d(B) = \left(\frac{(1 - \zeta^2(B))k_{eff}(B)}{m} \right)^{1/2} \tag{13}$$

It is observed that during transient oscillation of the nonlinear system, the response is similar to the decaying sinusoid seen in linear analysis. It is reasonable to assume that the motion of the nonlinear system from one extremum of oscillation to the next extremum is representable as the decay of a linear system over a half-cycle. As an example, we consider a system decaying from initial conditions of some initial displacement B_o and zero initial velocity. Let B_i denote the amplitude of the i^{th} extremum (occuring at time t_i) and B_{i+1} denote the amplitude of the next extremum (at time t_{i+1}). Then from linear theory, the time elapsed between one extremum and the next is approximately

$$\Delta t = t_{i+1} - t_i = \frac{\pi}{\omega_d(B_i)} \tag{14}$$

and the relationship between successive peaks is

$$B_{i+1} = - B_i \, e^{-\zeta_i \pi / (1 - \zeta_i^2)^{1/2}} \tag{15}$$

Given the initial amplitude B_o, we can efficiently estimate successive extrema and the time increments at which they occur from (14) and (15). Since the extrema occur each half cycle, we refer to this method as the Half-Cycle Method.

This Half-Cycle Method is an efficient way of approximating a numerical time integration to find extrema of transient oscillation. Numerical simulations of SDF systems show that this method is accurate for nonlinear systems in which $\epsilon = k_d/(k + k_d) \leq 0.5$ and provides a reasonable approximation for the amplitude of response for $\epsilon > 0.5$. The Half-Cycle Method results were compared to more accurate solutions generated by fourth order Runge-Kutta time integration. The comparison of the half cycle estimates to the numerically generated "exact" solutions is shown in Figures 2a-d where the Half-Cycle estimates of the extrema of response are shown as points (the exponential decay envelopes pictured are a result of the new Amplitude Averaging Method and will be discussed later). For nonlinearities of $\epsilon > 0.5$, the system experiences an offset that is not accounted for in the Half-Cycle Method. However, the peak-to-peak amplitude estimates are approximated reasonably well despite this offset. It may be observed that for these simulations this approach yields conservative estimates of system behavior in that it overestimates the amplitudes of response.

Amplitude Averaging Method

We now introduce a new linearization called the Amplitude Averaging (AA) Method. In this approach, the half-cycle values of damping and stiffness are averaged over the entire response range of interest. Consequently, while these average values are nonlinear functions of the initial displacement, they are constants as far as the transient response analysis is concerned.

The AA Method is also based on equations (3) through (6). Linear, constant parameters are derived by averaging c_{eff} and k_{eff} from (9) over the nonlinear range of oscillation, i.e.,

$$\bar{c}_{eff}(B_o) = c + \bar{c}_e(B_o) = c + \int_{x_{crit}}^{B_o} \frac{-F_s(B)}{B\omega}\, dB/(B_o - x_{crit}) \tag{16}$$

$$\bar{k}_{eff}(B_o) = k + \bar{k}_e(B_o) = k + \int_{x_{crit}}^{B_o} \frac{-F_c(B)}{B}\, dB/(B_o - x_{crit}) \tag{17}$$

where ω in (16) is given by (12). After averaging, (8) becomes

$$m\ddot{x} + (c + \bar{c}_e(B_o))\dot{x} + (k + \bar{k}_e(B_o))x = 0 \tag{18}$$

For the example of Coulomb friction, the analysis can be simplified by expressing the averaged properties in terms of several nondimensional parameters: (normalized quantities are denoted by a * superscript)

$$\bar{k}_e(B_o) = k_d\, \bar{k}_e^*(B_o^*) \tag{19}$$

$$\bar{c}_e(B_o) = \frac{c_o}{\bar{\omega}^*(B_o^*)}\, \bar{c}_e^*(B_o^*) \tag{20}$$

where

$$c_o = 2m\omega_o = 2(m\, k_d)^{1/2} \tag{21}$$

$$\bar{\omega}^*(B_o^*) = \left(\frac{k}{k_d} + \bar{k}_e^*(B_o^*) \right)^{1/2} \tag{22}$$

and

$$B_o^* = \frac{B_o}{x_{crit}} = \frac{B_o\, k_d}{\mu N} \tag{23}$$

$\bar{k}_e^*(B_o^*)$ and $\bar{c}_e^*(B_o^*)$ are the nondimensional averaged stiffness and damping of the friction element. These quantities are of particular interest because their values may be calculated in terms of the single nondimensional parameter, B_o^*, the initial displacement divided by the displacement required for slip to occur.

For Coulomb friction from (4), (17), and (19), $\bar{k}_e^*$ is given by

$$\bar{k}_e^*(B_o^*) = \frac{1}{\pi(B_o^* - 1)} \int_1^{B_o^*} \left\{ \theta(B^*) - 0.5 \sin[2\theta(B^*)] \right\} dB^* \tag{24}$$

where

$$\cos\theta(B^*) = 1 - \frac{2}{B^*}, \qquad (B^* \geq 1)$$

and need be calculated only once. The nondimensional frequency $\bar{\omega}^*$ is then obtained from (12), (17), and (19) as

$$\bar{\omega}^*(B_o^*) = \left(\frac{k}{k_d} + \bar{k}_e^*(B_o^*) \right)^{1/2} \tag{25}$$

Lastly, from (5), (16), and (20), the average nondimensional damping is approximated as

$$\bar{c}_e^*(B_o^*) = \frac{2}{\pi(B_o^* - 1)} \int_1^{B_o^*} \left\{ \frac{1}{B^*} - \frac{1}{(B^*)^2} \right\} dB^* \tag{26}$$

which, upon integration, yields

$$\bar{c}_e^*(B_o^*) = \frac{2}{\pi(B_o^* - 1)} \left\{ \frac{2}{B_o^*} + \ell n\,(B_o^*) - 1 \right\} \tag{27}$$

Note that the parameters are averaged only over the range in which they exhibit nonlinear behavior. The system is linear for B_o^* less than one and the response can be calculated using standard methods in that regime.

The AA Method gives a linear estimate of the nonlinear behavior of the system. Results from the AA linearized systems are shown in Figures 2a-d as exponential decay envelopes, and are plotted with the Half Cycle Method and Runge Kutta results

for comparison. As with the Half-Cycle Method, we again see conservative estimates of system amplitudes and again the estimates are more precise for weakly nonlinear systems.

An important result of the AA Method is shown in Figure 3. This figure shows the normalized quantities $k_e^*(B_o^*)$, $c_e^*(B_o^*)$, $\bar{k}_e^*(B_o^*)$, and $\bar{c}_e^*(B_o^*)$ in terms of the nondimensional initial displacement B_o^*. It is observed that there are optimal system configurations which maximize either instantaneous or average damping in the system. These optimality conditions depend only on the nondimensional initial displacement B_o^*. Recall from (23) that B_o^* is dependent on the system parameters. Thus, by adjusting just one of these parameters, say, normal load for example, it is possible to optimally damp an existing system. For example, the points A, B, and C on the average damping curve can be thought of as three systems which are identical except for the tightness of the friction joint as indicated by the normal load (normal load = N, $N_A > N_B > N_C$). Comparing the linear average damping terms provided by the AA Method for the three systems, it is seen that system B, with normal load N_B, has the highest value of average damping and is an optimally damped system for this set of basic parameters. The optimality of system B in an average sense was confirmed by fourth order Runge-Kutta simulations. The results for the three systems A, B, and C are shown in Figure 4, where successive extrema have been connected to form an envelope of decay. The normal load N_B is not simply the largest or smallest normal load which could be applied, nor is it equal to the load which would be required to optimally damp only the first oscillatory swing in the transient motion (this normal load would correspond to the conditions of system D of Figure 3 which maximizes instantaneous damping).

Runge-Kutta simulations confirm the optimality results which were readily provided by the AA Method. We observe, however, that the optimality result would not have been nearly so obvious if an exact time integration alone had been used to investigate this transient behavior. It is also noted that the AA Method provides general results in that it allows for parameter-based comparisons of different systems. Numerical time integration methods lack this generality, yielding instead results which are case-specific and thus more difficult to interpret when comparing systems.

The AA Method leads to systems which are optimized, in an averaged sense, over the entire range of nonlinear behavior. The Half-Cycle Method may be used to generate systems which are optimal in a "first swing" sense. It is also possible to

optimize the system over other select ranges of nonlinear behavior. This is done by averaging the c_{eff} and k_{eff} equations over the particular range of concern, resulting in a new curve for $\bar{c}_e^*(B_o^*)$. The optimal normal load (or other parameter) is the one which adjusts the nondimensional initial condition so as to maximize the value of this new $\bar{c}_e^*(B_o^*)$. The linearizations described so far make it possible to optimize the nonlinear system, in an average sense, over any range of nonlinear behavior.

The Amplitude Averaging Method has yielded a general result which was not obvious from numerical time integrations. In the next section, the application of the AA Method to multiple mass systems is developed and it is shown that the principles of generality-of-results and optimal damping still apply, only that they now apply in a modal sense.

Multiple Degree of Freedom Systems

The transient analysis of multiple-degree-of-freedom (MDF) nonlinear systems using the AA Method can be accomplished by representing the system in modal form in terms of a sum of SDF nonlinear systems. The SDF components are linearized separately and are then combined to form a linear representation of the MDF system.

In the linearization process, a nonlinear friction damper will be replaced by linear elements which approximate its behavior, as depicted in Figure 5. The original 2DF system incorporates a friction damper as a nonlinear element and will serve to illustrate the application of the Amplitude Averaging Method to MDF nonlinear systems. The equations of motion for the system may be written in matrix form as

$$\mathbf{M}\ddot{\mathbf{x}} + \mathbf{C}\dot{\mathbf{x}} + \mathbf{K}\mathbf{x} = -f_n \begin{bmatrix} 1 \\ -1 \end{bmatrix}$$

where

$$\mathbf{x} = \begin{bmatrix} x_1 \\ x_2 \end{bmatrix}$$

$$\mathbf{M} = \begin{bmatrix} m_1 & 0 \\ 0 & m_2 \end{bmatrix}$$

$$C = \begin{bmatrix} c_1 & 0 \\ 0 & c_2 \end{bmatrix}$$

$$K = \begin{bmatrix} k_1 + k_3 & -k_3 \\ -k_3 & k_2 + k_3 \end{bmatrix}$$

MDF Linearization

In the SDF analysis we were able to regard the initial amplitude across the friction damper as the maximum distance that the joint would be stretched during transient oscillation. In the MDF system, the initial amplitude across the joint is no longer guaranteed to be the maximum span which the joint experiences. Consequently, the nonlinear system cannot be linearized by simply considering the isolated friction damper and how much it is initially displaced. Instead, one must use a modal approach in the linearization process.

It is necessary to decouple the nonlinear MDF system of Figure 5 into two SDF nonlinear systems so that the AA Method may be applied to each of the decoupled systems separately. Decoupling of linear systems is done routinely (see, for example, Thomson [7]) while nonlinear systems are not generally amenable to such analysis. The nonlinear decoupling and modal linearizations may be accomplished with the iterative approach summarized in Appendix A. In this approach, a set of converged eigenvalues and eigenvectors is obtained and used to form a modal (decoupled) representation of the nonlinear system. The decoupled systems are linearized using the AA Method and are transformed back to the original coordinates to yield a linear MDF system.

Several approximations are made during the decoupling process. Viscous damping is generally small and is, therefore, neglected in order to avoid the inconvenience of dealing with complex eigenvectors. The complex formulation could be pursued in order to increase the overall accuracy of the linearization and estimation scheme. Another assumption made in the analysis is that each modal friction joint operates independently. This approximation significantly simplifies the calculations, but introduces an additional source of error in those cases where modes interact. This latter assumption is believed to be responsible for the fact that the modal AA response estimates are no longer conservative in some instances.

However, in general the results obtained from the AA Method compare reasonably well with results from direct time integration. The modal comparisons for two cases are shown in Figures 6 and 7. where the time integration solutions have been transformed from the original x coordinates into the converged modal coordinates, y_1 and y_2, by using the converged eigenvectors. Overall, the exact modal solutions (represented by the continuous curves) are seen to be similar in form to decaying sinusoids centered about a zero equilibrium state. The neatness (symmetry and sinusoidal appearance) of the exact results indicate that the converged linear decoupling does in fact represent the nonlinear behavior fairly well, as the response in x coordinates would transform poorly if the modal representation were not a reasonable estimate of system response.

Several characteristics of the AA Method as applied to MDF systems are illustrated in Figures 6, 7, and 8. Firstly, the AA estimates are not conservative in the lowest mode when both modes are actively slipping.[2] Secondly, it was found that the larger the viscous damping and nonlinearities in a mode, the less "neat" the modal response looks (this is apparent in Figures 7b and 8b). Thirdly, a MDF system can be modally optimized in a fashion similar to that used to optimize the SDF system. As in the SDF case, the correct manipulation of the normal load shifts the nondimensional modal initial condition to a condition which generates the optimal (modal) damping. It is noted that it is not generally possible to optimally damp both modes simultaneously, as the optimization of one mode results in a detrimental or non-optimizing shift of the other mode. Figure 6 shows a system which is not optimally damped in either mode. Figure 7 shows the same system after the normal load has been adjusted to optimally damp the higher frequency mode (mode 2). Notice that the results are plotted on different scales in Figures 6 and 7. In Figure 8b, the extrema in the numerical time integration solutions for the non-optimized-mode 2 and optimized-mode 2 systems have been scaled for direct comparison (extrema plotted to form decay envelope). From Figure 8b it is obvious that the optimization has a significant effect on modal response. The same system was optimized in mode 1 and the results depicted in Figure 8a. Note that in this particular system the friction damping in the first mode was quite small compared to viscous damping and, consequently, optimizing joint damping had little impact on first mode response (an expanded scale was used to show the optimization result more clearly). The AA optimization results for both modes 1 and 2 were confirmed by Runge-Kutta

[2] It was found that if only one mode was actively slipping the accuracy of the AA method for MDF systems was comparable to that found for SDF systems.

simulations. Thus, although the modal AA extrema may be nonconservative in some cases, the AA indication of modal optimality remains accurate in the cases considered.

The AA Method may thus be used to optimally damp select modes of particular concern. This is helpful in the design process in that it gives an easy indication of which systems are optimal in a given situation. In practice it may not be possible to obtain joints with characteristics that exactly correspond to this modeled optimality, in which case the issue may become one of selecting the most nearly optimal joint configuration from a variety of available designs.

Conclusion

This paper has discussed the specific application of the Amplitude Averaging Method to friction damped systems. However, the AA Method is a general linearization method applicable not only to friction damped systems but also to other systems which exhibit nonlinear hysteretic behavior.

The AA Method is efficient and can be used to easily establish optimization conditions, subject to time integration verification. Familiar modal analysis may be applied to MDF nonlinear systems and systems may be optimized over specific ranges of nonlinear oscillation. Furthermore, the AA Method can be used to modally optimize MDF systems in order to suppress system response over specific frequency ranges.

The AA Method may also be used as a comparison tool in the system design process. The physical parameters of the system may not be adjustable to the indicated optimal values. For example, in the case of jointed structures and friction damping, it is not generally possible to select physical joints with adjustable (optimizable) normal loads. In this situation the task may be one of selecting joints from a variety of designs. The AA Method yields the relative averaged damping in these designs for amplitudes of response which are representative of those encountered in practice and thus may be employed as a method of comparison in order to help choose the most nearly optimal design.

The AA Method is an efficient design tool for two reasons. One is that the method is computationally efficient. In the cases considered in this paper, AA solutions could be calculated an order of magnitude more quickly than numerical time integration solutions. In addition, the method provides a system representation in

terms of linearized modes and, consequently, it becomes relatively easy to establish optimum system response. Again, it is our view that numerical time integration and the AA Method are complimentary approaches and that both have their places in the design of nonlinear systems. The AA Method is a computationally efficient approach which supplies analytical insight at the expense of accuracy, while the computationally intensive time integration approach provides verification and fine tuning of the results for select cases of interest.

References

1. Hughes, Thomas J. R., *Finite Element Method*, Prentice-Hall, New Jersey, 1987.

2. Iwan, W. D. and Gates, N. C., "Estimating Earthquake Response of Simple Hysteretic Structures," *Journal of the Engineering Mechanics*, AJCE, Vol. 105, No. EM3, June 1979, pp. 391-405.

3. Sinha, A., and Griffin, J. H., "Effects of Static Friction on the Forced Response of Frictionally Damped Turbine Blades," *ASME Journal of Engineering for Gas Turbines and Power*, Vol. 106, Jan. 1984, pp. 65-69.

4. Caughey, T. K., "Sinusoidal Excitation of a System With Bilinear Hysteresis," ASME Journal of Applied Mechanics, Vol. 27, 1960, pp. 640-643.

5. Crawley, Edward F., "Identification of Nonlinear Structural Elements by Force-State Mapping," *AIAA Journal*, Vol. 24, No. 1, Jan. 1986, pp. 155-162.

6. Menq, C.-H., and Griffin, J. H., "A Comparison of Transient and Steady State Finite Element Analyses of the Forced Response of a Frictionally Damped Beam," *ASME Journal of Vibration, Acoustics, Stress, and Reliability in Design*, Vol. 107, Jan. 1985, pp. 204-210.

7. Thomson, William T., *Theory of Vibrations With Applications*, Second Ed., Prentice-Hall, New Jersey, 1981, pp 132-201.

Acknowledgements

This work was supported by NASA Langley Research Center, Grant No. NAG-1-612-NA64, under the direction of Mr. Lucas Horta.

A. ITERATIVE METHOD FOR DECOUPLING AND LINEARIZING A NONLINEAR MDF SYSTEM

The goal here is to represent the friction joint by equivalent linear elements for a given set of initial displacements. To this end we must find a modal representation of the friction element which depends (as in the case of the SDF system) on the initial modal displacements. It is not possible, however, to calculate the mode shapes or eigenvectors of the system and find the initial modal displacements unless we know all the stiffnesses of the system (including those of the friction joint). This appendix summarizes an iterative procedure for simultaneously establishing the eigenvectors and initial modal displacements of the system and the equivalent joint properties of the friction element.

This method neglects damping in determining the eigenvectors of the system. This is a reasonable approximation for lightly damped systems. There are seven steps in the process, which are illustrated by applying them to the two-degrees-of-freedom (2DF) system of Figure 5.

1. Write the governing equation of the system in matrix form, neglecting viscous damping, e.g., for the 2DF system of Figure 5

$$M\ddot{x} + K_o x = f_n \begin{bmatrix} -1 \\ 1 \end{bmatrix} \tag{A.1}$$

where $K_o = K$.

2. Find the eigenvalues and eigenvectors of the linear part of the system, momentarily disregarding the nonlinear term f_n. Form the matrix of eigenvectors, U, e.g.,

$$K_o u_i = \lambda_i M u_i \qquad \text{eigenvalues } \lambda_1, \lambda_2$$

$$\text{eigenvectors } u_1 = \begin{bmatrix} u_{11} \\ u_{21} \end{bmatrix} \qquad u_2 = \begin{bmatrix} u_{12} \\ u_{22} \end{bmatrix} \tag{A.2}$$

$U = [u_1, u_2]$ ... matrix of eigenvectors.

3. Assume x can be represented in terms of modal coordinates $y = (y_1, y_2)^T$, i.e.,

$$x = Uy \tag{A.3}$$

then

$$y = U^{-1}x$$

The modal initial conditions can be found using (A.3) and the orthogonality of the eigenvectors (with respect to **M**)

$$y_o = U^{-1}x_o$$

4. Using $x = Uy$ in (A.1) yields

$$MU\ddot{y} + K_o Uy = f_n \begin{bmatrix} -1 \\ \\ 1 \end{bmatrix}$$

$$U^T MU\ddot{y} + U^T K_o Uy = U^T f_n \begin{bmatrix} -1 \\ \\ 1 \end{bmatrix}$$

5. Find linearized stiffnesses for each independent mode using the AA method. This step yields

$$U^T MU\ddot{y} + U^T K_o Uy = - K_q y - C_q \dot{y}$$

(Analogous to:

$$- f_n = - \frac{F_c}{B} x + \frac{F_s}{\omega B} \dot{x} \Rightarrow - k_e x - c_e \dot{x}$$

as done in the SDF case in equations (7,8,16,17,18) in the main body of the paper.) K_q is a diagonal matrix, each diagonal element is the linearized stiffness of the friction element in its respective mode, e.g., in the example 2DF system, slip occurs when

$$\mu N = k_d(x_1 - x_2) = k_{d_1} y_1 + k_{d_2} y_2$$

where

$$k_{d_i} = k_d u_i \ [1,-1]$$

Assume that slip occurs independently in each mode. Then the modal displacement required for slip is

$$y_{i_{crit}} = \frac{\mu N}{k_{d_i}} \text{ (analogous to } x_{crit} = \frac{\mu N}{k_d})$$

The modal initial conditions were found in Step 3. Given the initial conditions and the slip conditions, the AA method may be applied to each mode separately in order to linearize the decoupled systems. From the first mode, the linearized stiffness term is $-k_{e_1}$. Mode 2 yields $-k_{e_2}$.

Form K_q: $K_q = \begin{bmatrix} k_{e_1} & 0 \\ 0 & k_{e_2} \end{bmatrix}$

The linearized modal stiffnesses have been found (C_q is found simultaneously but not used at this point in the analysis).

6. Convert back to original coordinates:

$$x = U^{-1}y$$

Substituting into the linearized governing equation from Step 5:

$$M\ddot{x} + K_o x = - U^{T^{-1}} K_q U^{-1} x \quad \text{(neglect } C_q\text{)}$$

define

$$K_{mod} \cong U^{T^{-1}} K_q U^{-1}$$

then

$$M\ddot{x} + (K_o + K_{mod})x = 0$$

7. $K_1 = K_o + K_{mod}$, then

$$M\ddot{x} + K_1 x = 0$$

But this system has different eigenvalues and eigenvectors than the original system considered in Step 2. The linearization of Step 5 was dependent on the eigenvectors of the system, which have changed after linearization. To obtain a more accurate linearization, repeat Steps 1-7 using the eigenvectors from the M_1, K_1 system.

The process (Steps 1-7) may be repeated as many times as needed to obtain a converged set of eigenvectors using $M, K_{(i)}$. In practice, this method usually converged in four iterations and never required more than six iterations.

While the linearized damping can be readily calculated at any iteration, it is neglected along with any original viscous damping in estimating the eigenvectors of the system. For this reason, the method is less accurate when high viscous damping or large nonlinearities are present in the system. A complex eigenvalue and eigenvector approach could be used to improve the accuracy when the damping terms are large.

In the current approach the equivalent linear damping from the friction joint is calculated for each mode only after the eigenvectors have fully converged. This is added to the modal viscous damping to establish the total effective damping (analogous to (16)) for each mode. The response of each mode is then calculated in the same manner as for a linear single degree of freedom system to obtain the comparisons indicated in Figures 6 and 7. The physical displacements may be readily calculated from (A.3).

Figure Captions

Figure 1 Single Degree of Freedom System.

Figure 2 Comparison of Results for $m = k + k_d = \mu N/k_d = 1$ and $c = 0.02$.

Figure 3 Instantaneous and Average Values of Stiffness and Damping.

Figure 4 Response Envelopes Indicate Optimum Damping.

Figure 5 Schematic of Linearization Process.

Figure 6 Modal Response of MDF System: $k_1 = k_3 = m = 1$, $k_2 = 2$, $c_1 = c_2 = 0.01$, $k_d = 0.25$, and $\mu N = 0.1$.

Figure 7 Modal Response When Second Mode Optimally Damped: μN Changed to 0.35.

Figure 8 Comparison of Modal Response Envelopes.

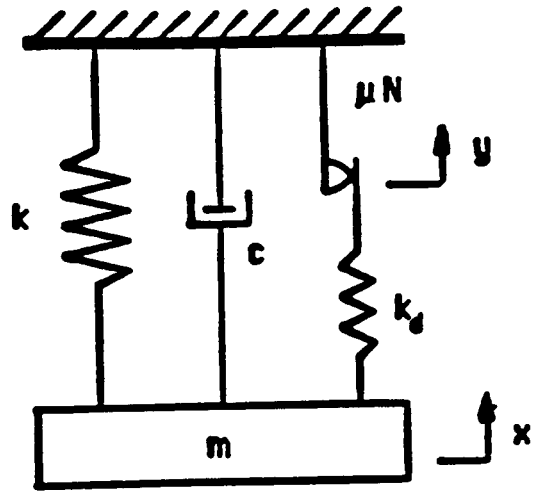

Figure 1a

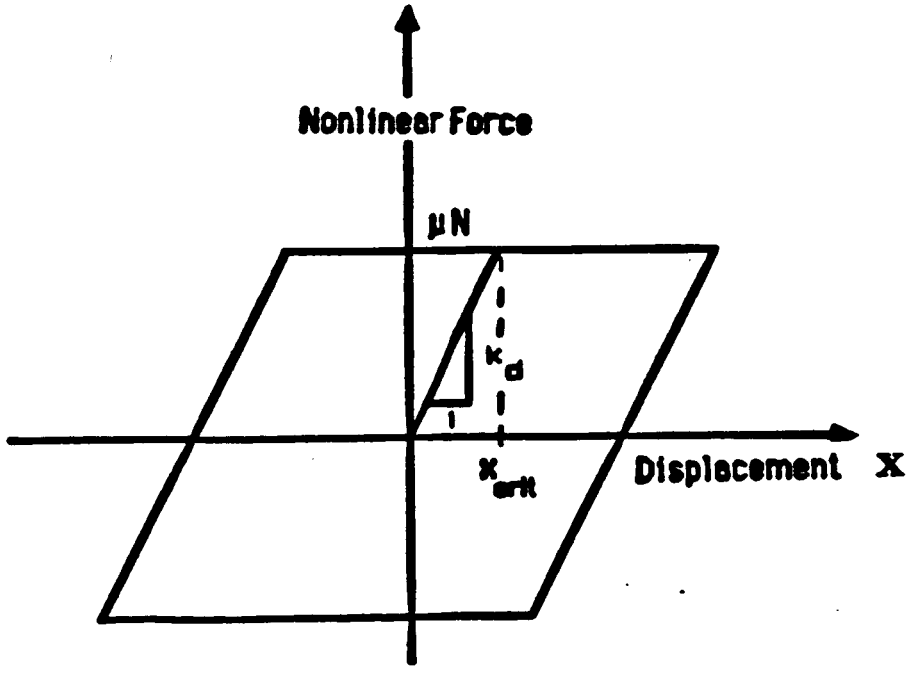

Figure 1b

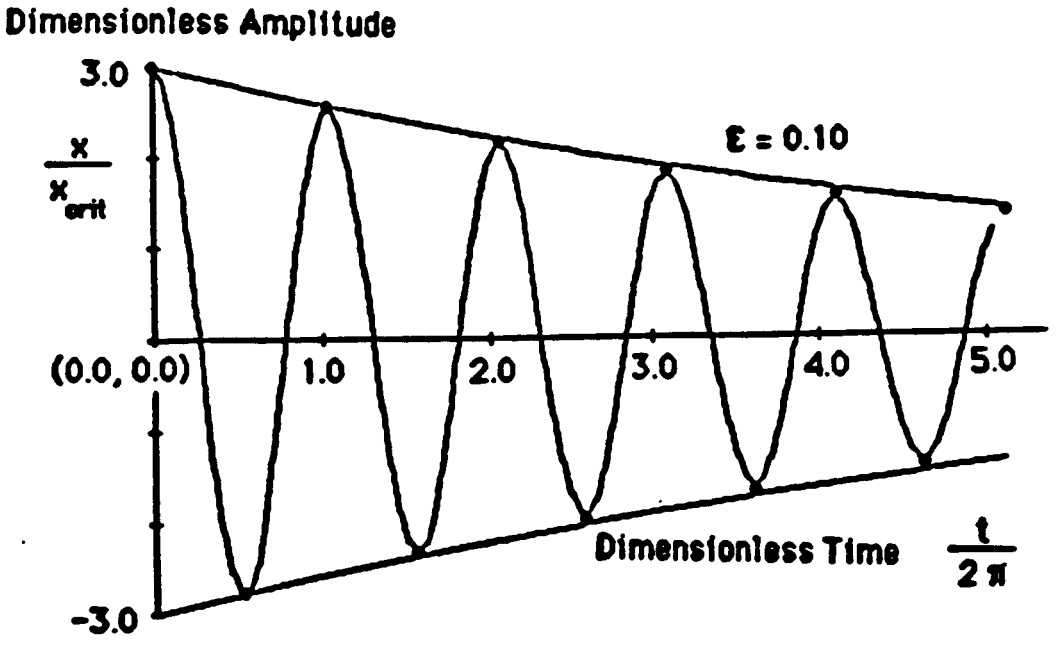

Figure 2a

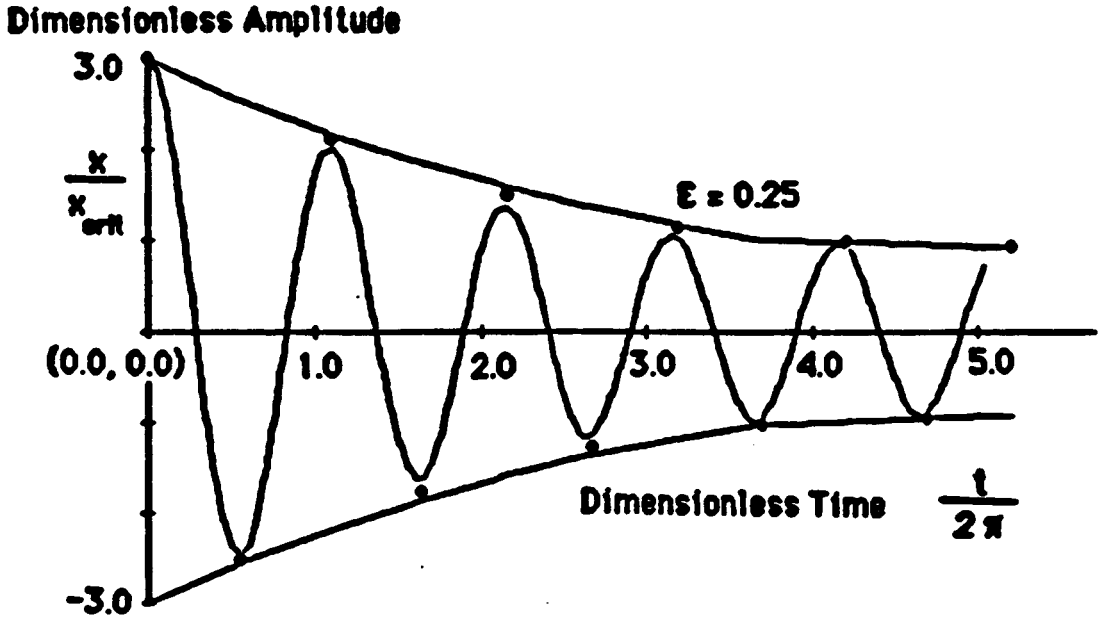

Figure 2b

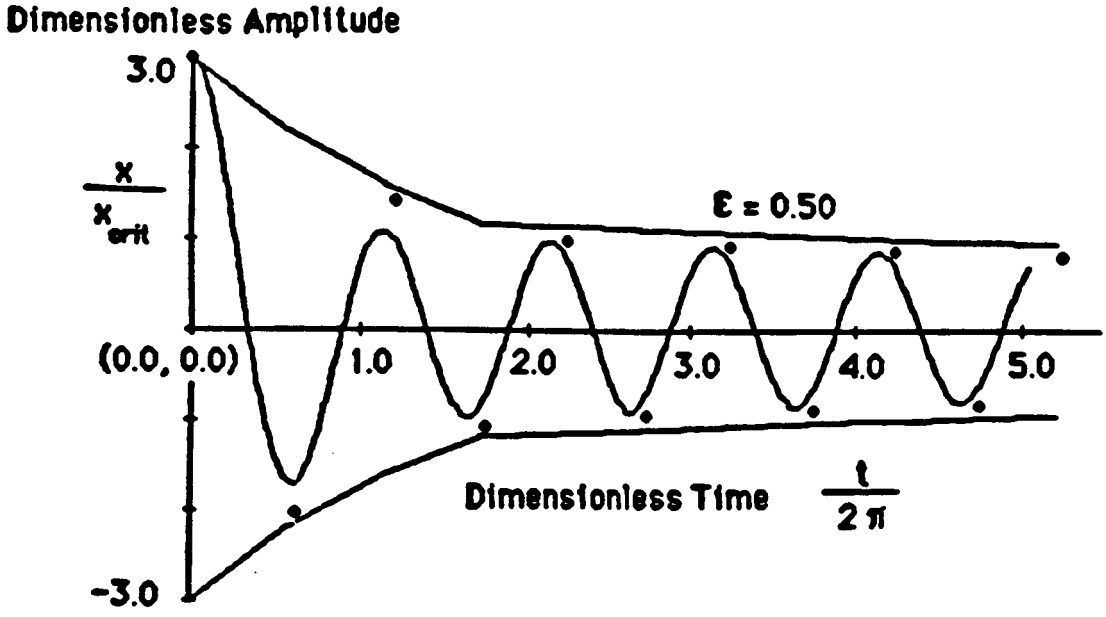

Figure 2c

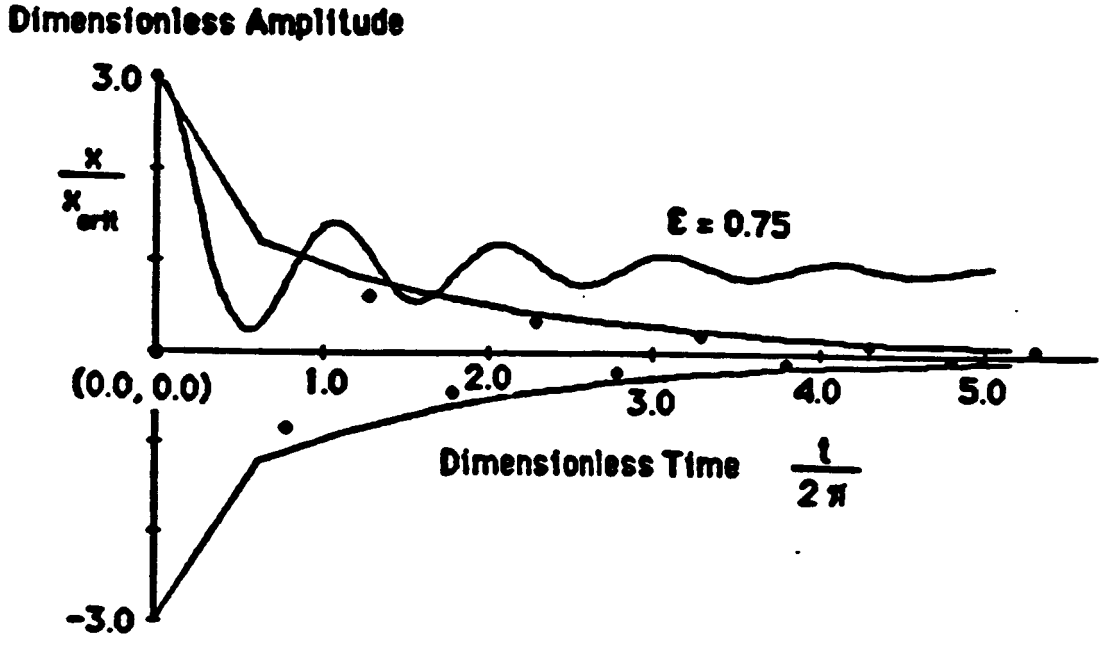

Figure 2d

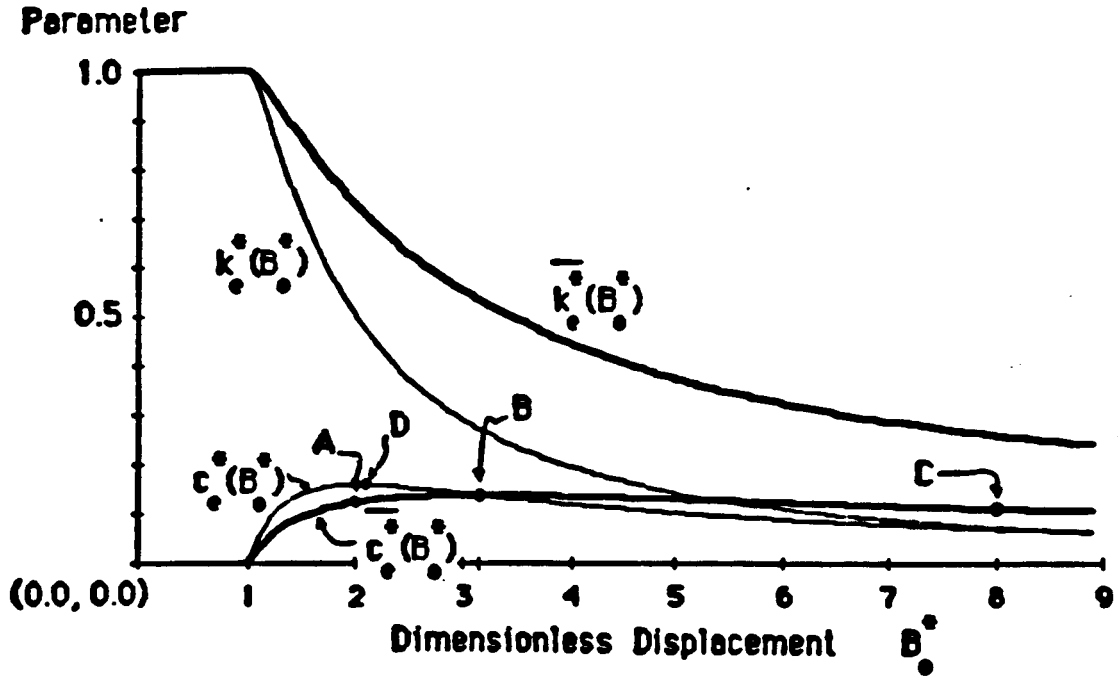

Figure 3

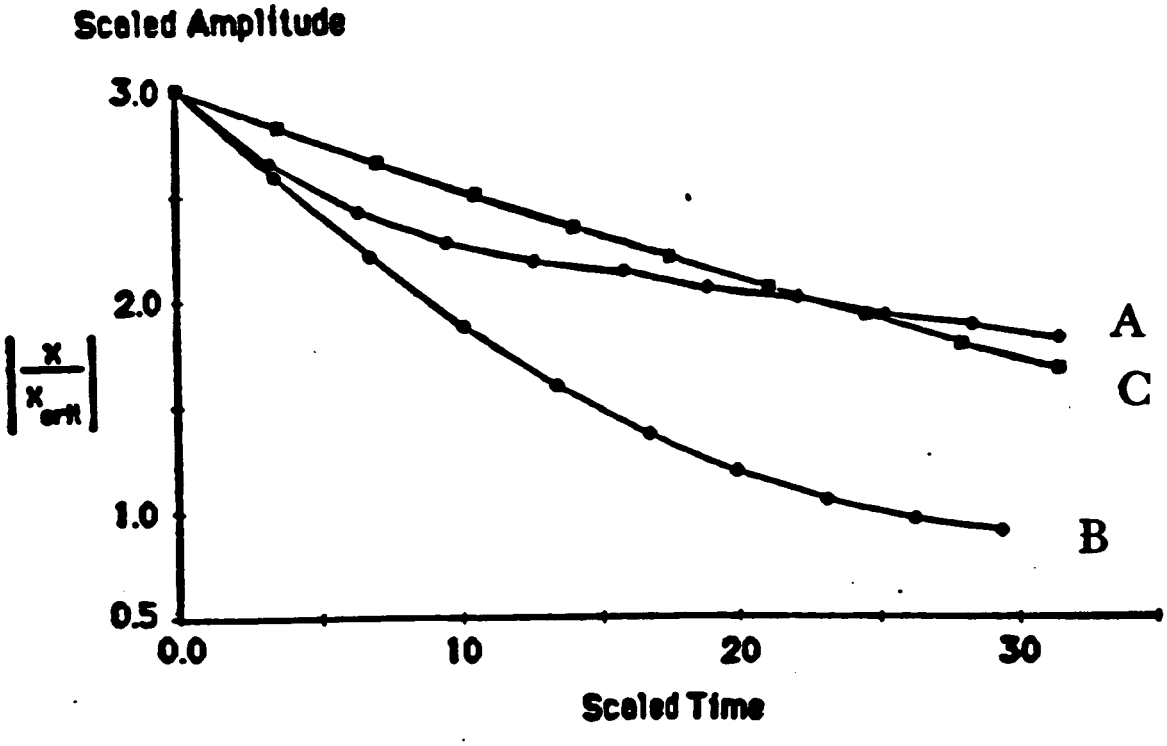

Figure 4

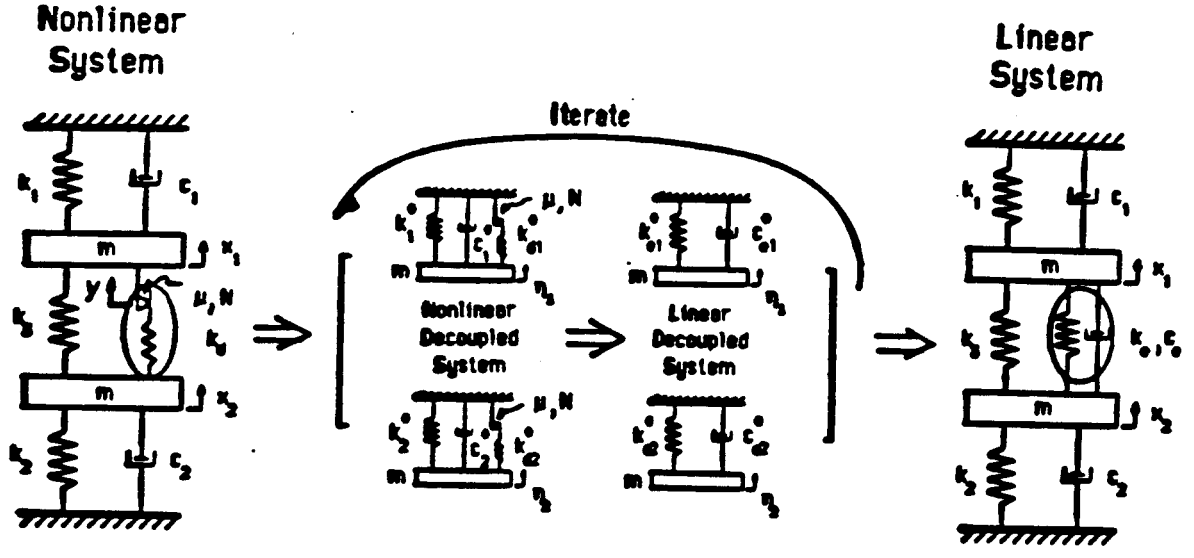
Nonlinear System
Iterate
Linear System
Nonlinear Decoupled System
Linear Decoupled System

Figure 5

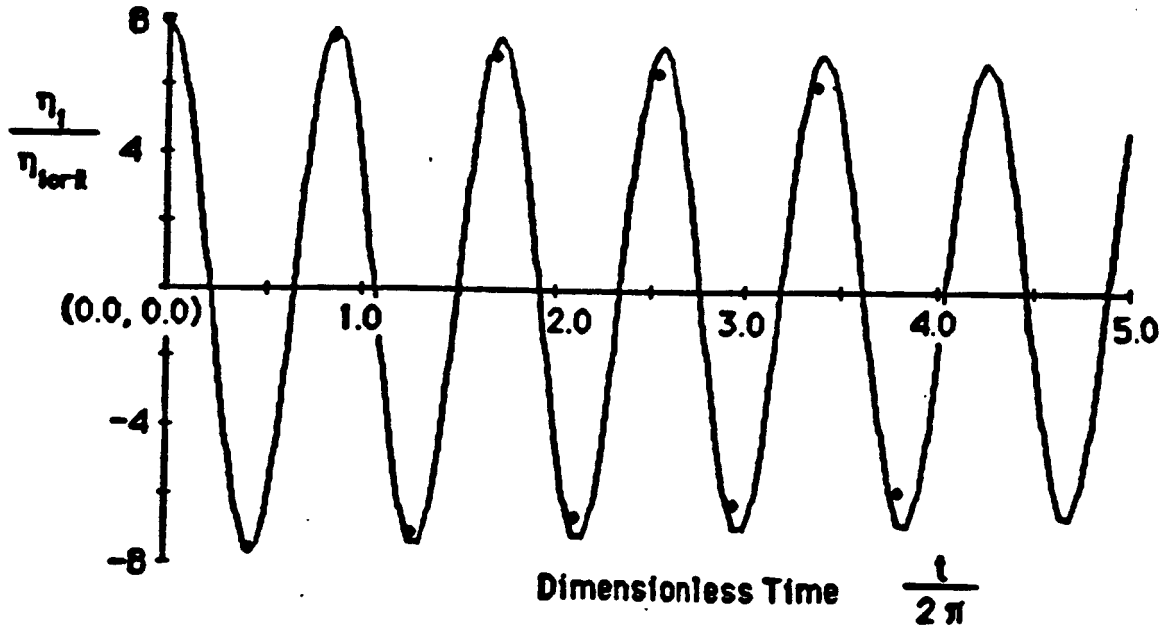

Figure 6a

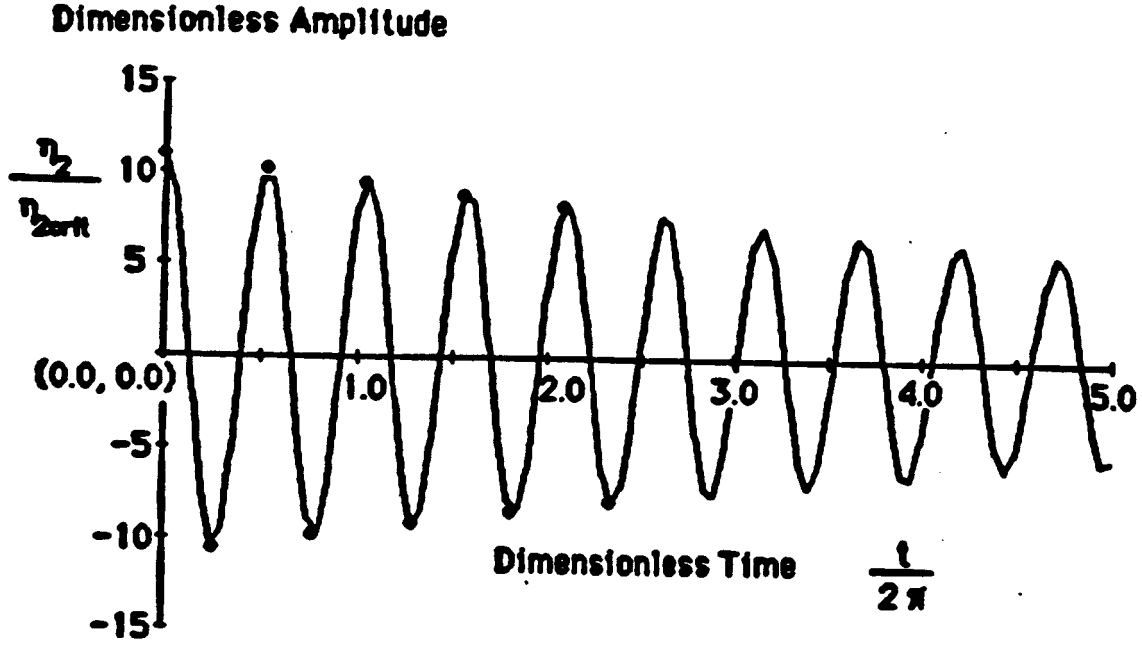

Figure 6b

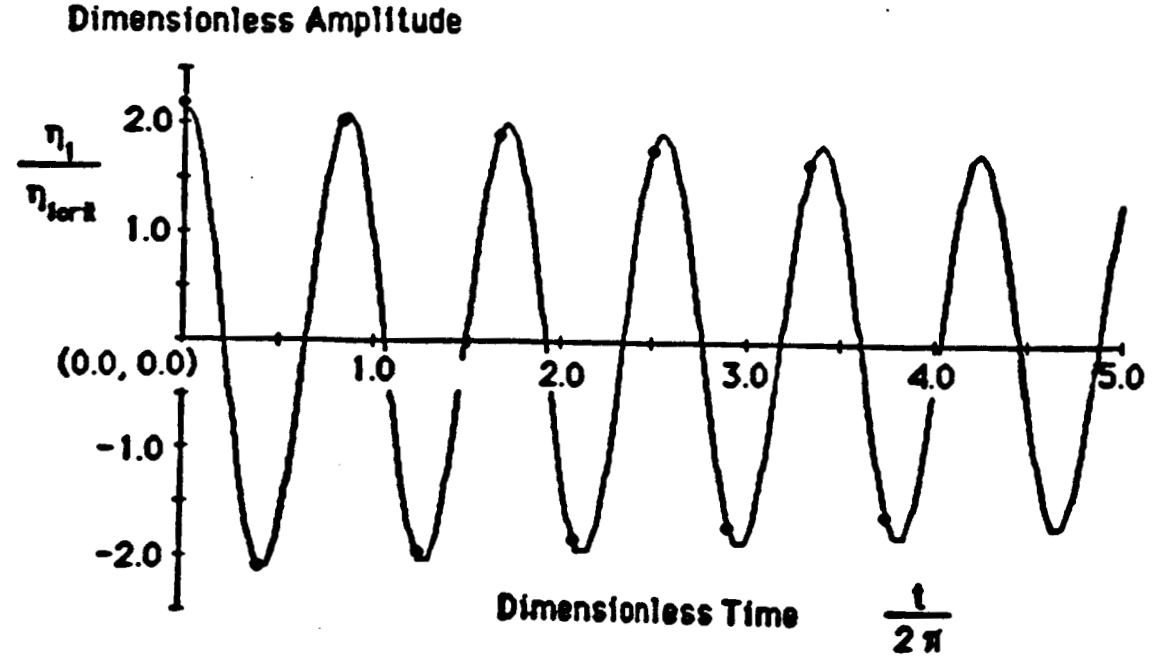

Figure 7a

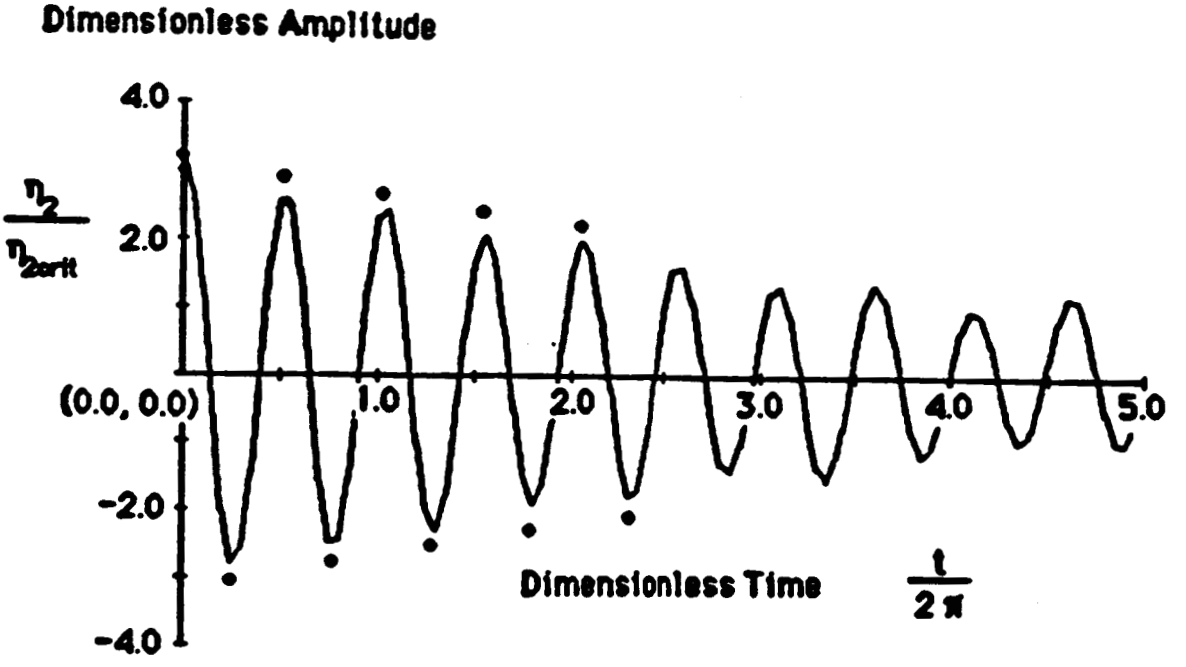

Figure 7b

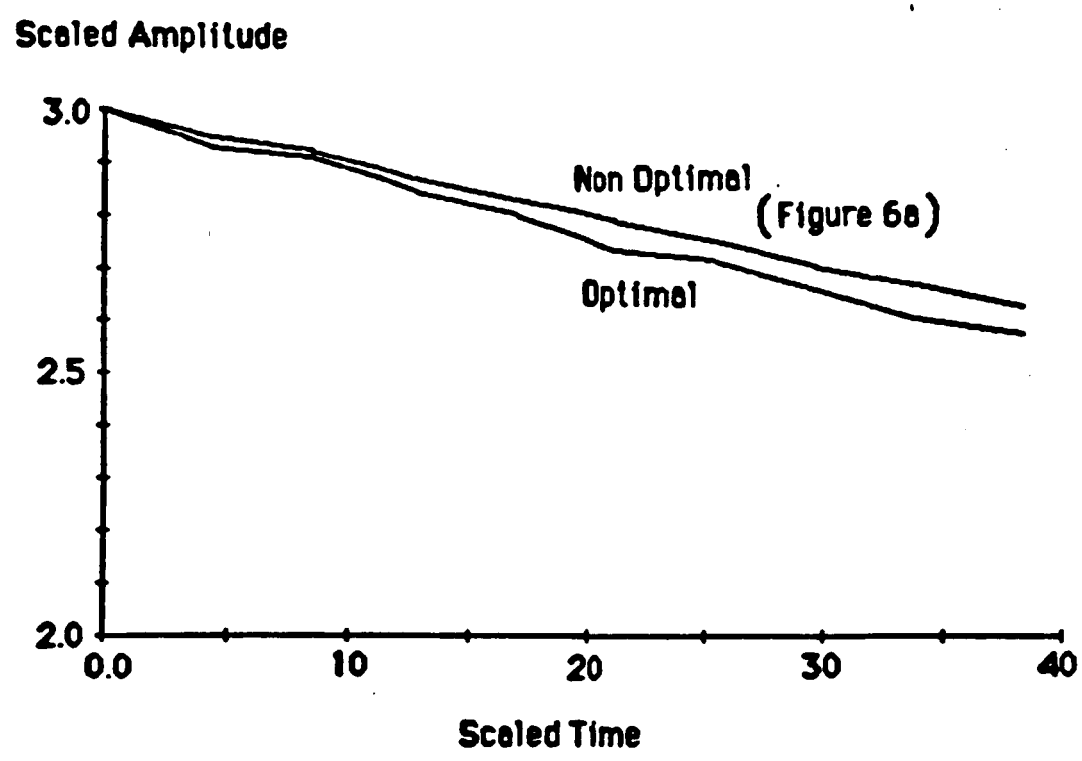

Figure 8a

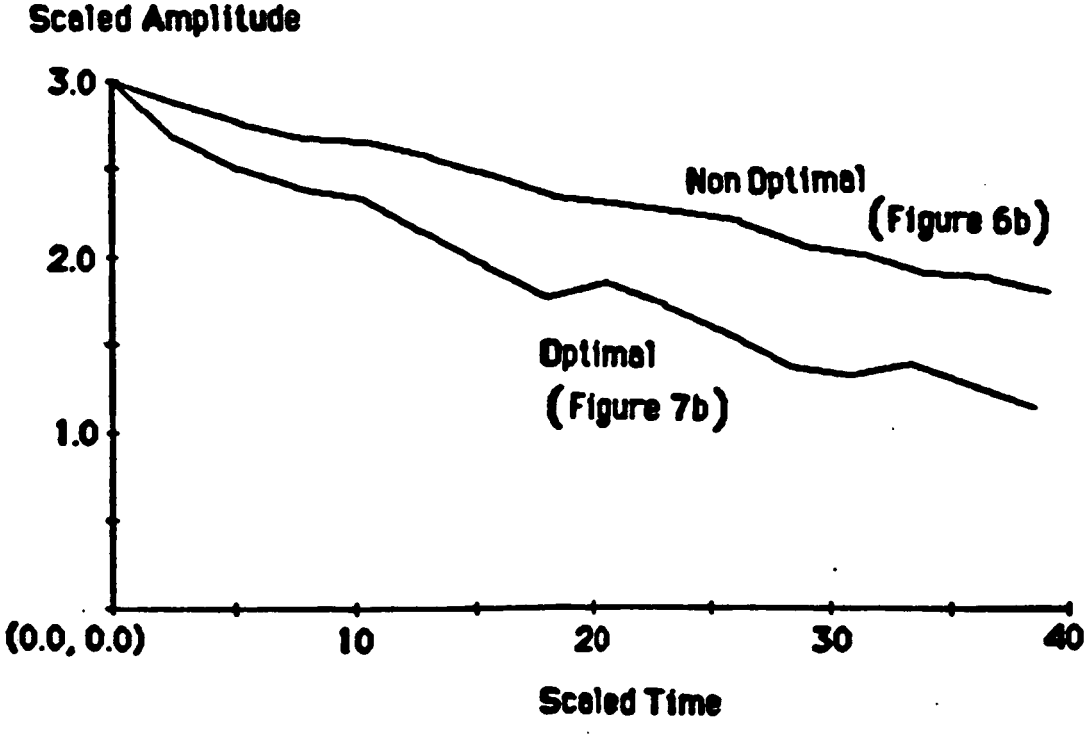

Figure 8b

3. How Gravity and Joint Scaling Affect Structural Response

Shyr-Tzer Hsu
J. H. Griffin
J. Bielak

Carnegie Institute of Technology
Carnegie Mellon University
Pittsburgh, PA 15213

Table of Contents

1. INTRODUCTION

Many engineering structures are subjected to motions in which limited slip can occur between members. This is frequently the case for bolted and riveted structures and can also occur in joints found in space applications. Truss structures designed for space often are constructed with joints that can rotate and lock into place. This allows the structure to collapse into a compact package that is easily transported to space and then expanded. Typically, this type of joint mechanism is subject to limited slip behavior because of "slop" due to machining tolerances. In addition, joint slip is usually constrained by friction forces within the mechanism. This means that the joint's motion is controlled by friction until it reaches the end of the free play and then it is constrained elastically. This type of nonlinear behavior can have a strong influence on system response. In particular, because of the limited slip or the 'gap' aspect of the joint behavior scaled models of the jointed structure may not respond dynamically in the same manner as the full scale structure in space. This may be the case for two reasons.

The first reason that a scaled model of a structure may not have the same dynamic response is that tolerances in the joints are not scaled. Typically, engineers wish to have joints that behave as linearly as possible. Consequently, when they are designing the full-scale joint they stipulate as small tolerances as possible to reduce slop and the associated nonlinear behavior. When sub-scale models of the joint are developed for testing, the same absolute tolerances are stipulated since they cannot be further reduced. As a result, the free-play in the sub-scale joints is, on average, significantly greater than in full-scale joints and the model structure will exhibit stronger nonlinear behavior.

A second reason that a scaled model of a structure may behave differently is that it may be tested under gravitational loading that does not occur in space. While there are laboratory procedures for supporting two dimensional structures (i.e. structures that have modes in which the motions lie in a plane) in such a way as to negate gravitational effects, they are not readily applicable to more complex, three dimensional structures. As a result, it is in general not possible to eliminate gravitationally induced preloads in the joint. The preload introduces a static displacement in the joint that tends to eliminate the free-play in one direction. Thus, for

example, the joint may behave elastically in the direction of the applied preload, and slip only when motion occurs in the opposing direction (in contrast to a joint without any static loads that slips in both directions). As a result, from a dynamics point of view, a joint with preloads tends to be effectively stiffer and contributes less damping to the system. A goal of the current research is to gain a better understanding of this effect.

This research considers the dynamic response of the lumped parameter system depicted in Figure 1. The system may be viewed as either a model of a single degree of freedom oscillator or a single mode representation of a general structural system as characterized by a given modal mass, stiffness and damping. The nonlinear element that represents the joint is indicated by the linkage having the spring stiffness k_d. In this linkage the friction element can slide once the magnitude of the force builds up to μN. Slip at the friction contact point is limited by the stops located at distances δ_1 and δ_2 and the total gap is given by δ. The system is subjected to a sinusoidal excitation and a static preload f_1. This system was chosen for examination because it is the simplest system which exhibits the characteristics of interest and yet, in a modal sense, has implications to a broad class of systems. To date we have concentrated on understanding the steady-state response of this system.

The steady-state response of the system is important for two reasons. The first is that it is easier to analyze than the transient response and, consequently, it is easier to establish important nondimensionalized system parameters. Since these parameters control transient response as well as steady-state response the final issue is how much they change in going from a full-scale to a sub-scale system. For example, one suspects that static preloads have little effect when the system's response is large since the amount of energy dissipated by friction is then independent of the static loads. This can be readily quantified by analyzing the system's steady-state response to establish for what range of dimensionless parameters this is true. This analysis is easier to perform for steady-state response because well established techniques (the describing function approach) exist for determining approximate solutions. The resulting analytical solutions are superior to numerical simulations because they are easier to compute and more general. Secondly, it has been shown in other work recently performed at Carnegie Mellon that the steady-state

behavior of a system can be used to estimate its transient response. Thus, it is clear that gaining an understanding of the factors that control the steady state response also has a direct bearing on how it will behave in the transient regime.

Iwan has analyzed a similar limited slip system in [1]. It differs from that considered here in that it did not contain the spring with stiffness k (refer to Figure 1) nor did he consider static preloads. Both of these factors are important in space applications.

2. ANALYSIS

The solution approach is explained in this section. In Part 1, the governing equation for the system is described. Its normalized form is given to provide a basis for parametric studies. The approximate method is introduced in Part 2, and the equations for calculating the frequency response are derived. Part 3 presents the procedures for obtaining the resonant responses. Part 4 shows how the frequencies and amplitudes where the vertical jumps occur are obtained. The procedures described in these sections provide an approach for understanding the unstable response phenomenon discussed in the latter sections.

2.1. Formulation of Governing Equations

The equation of motion for the system shown in Figure 1 is,

$$m\ddot{x}(t)+c\dot{x}(t) + k\,x(t) = f_o\cos\omega t + f_1 - f_n(x,\delta_1,\delta_2) \qquad (1)$$

where f_1 is the static load, and f_n is the nonlinear friction force at the joint.

The contact pressure on the joint, N, is assumed constant, and the inertia of the friction element is neglected. Therefore, f_n is constant throughout the length of the friction element.

The friction element will slide once the magnitude of the nonlinear force f_n equals N multiplied by μ, the friction coefficient of the materials in contact.

The nonlinear force f_n is a function of the mass displacement x. When $|x| \le \frac{\mu N}{k_d}$, where k_d is the stiffness of the friction element, the system is linear. When $|x| \ge \frac{\mu N}{k_d}$, and the stop distances δ_1, δ_2 are sufficiently large, the system has elasto-plastic behavior. When the stop

distances, δ_1 , δ_2 are not large enough, the system experiences a sudden hardening phenomenon. If the mass displacement x is periodic, several different hysteresis cycles of f_n vs. x can be drawn, as shown in Figures 2-6 (In the figures, A is the amplitude of the steady-state vibration and B is the static offset).

To render a foundation for the parametric study, equation 1 can be converted into a nondimensional form as shown below

$$d^2\bar{x}/d\bar{t}^2 + \zeta\, d\bar{x}/d\bar{t} + \bar{x} = \cos\bar{\omega}\bar{t} + \lambda_1 - \lambda_2 F(\bar{x}, \delta_2/\delta_1) \qquad (2)$$

Where,

$$\bar{x} = x/x_o \quad \text{and} \quad x_o = f_o/k$$

$$\bar{t} = t/t_o \quad \text{and} \quad t_o = \sqrt{m/k}$$

$$\lambda_1 = f_1/f_o \quad , \quad \zeta = c/\sqrt{mk}$$

$$\lambda_2 = \mu N/f_o \quad , \quad \bar{\omega} = \omega/t_o$$

As can be seen, the nondimensional scales are unities if the quantities m, k, f_o were set to unity. This fact is adopted in the sections below as a way to present general results.

One purpose of this study is to understand the steady-state response of the system shown in Figure 1. Although this task can be accomplished by solving equation 1 numerically for a sufficiently long period of time, such an approach is inefficient and computationally expensive. Therefore, an alternate, more efficient method is developed. The direct, long time solution is then used only to verify the accuracy of the analytical results in certain representative cases.

2.2. Approximate Method

Based on the fact that the excitation is periodic; we assume that the response is also periodic. Therefore, the displacement x can be expanded by Fourier series. In the steady-state, the response is approximately harmonic, i.e.

$$x = A\cos\theta + B \quad , \text{ where } \quad \theta = \omega t - \psi \qquad (3)$$

In the above, the offset term B is included to compensate for the shift due to the static load f_1.

The method used here was adopted in several earlier papers [1] [2] [3] that studied the friction damping of structures. Since the nonlinear force f_n depends on the oscillation of displacement x, it is also harmonic and can be linearized by representing it in terms of a truncated Fourier series as shown below.

$$f_n = f_b + f_c \cos\theta + f_s \sin\theta \tag{4}$$

Where

$$\begin{aligned} f_b &= \mu N F_b(\alpha, \beta, \gamma, q) \\ f_c &= \mu N F_c(\alpha, \beta, \gamma, q) \\ f_s &= \mu N F_s(\alpha, \beta, \gamma, q) \end{aligned} \tag{5}$$

In the above, F_b, F_c, F_s are nondimensional Fourier coefficients established in the Appendix and α, β, γ and q are dimensionless parameters also established in the Appendix (see equation 43).

It is noted that since the dynamic displacement is proportional to $\cos\theta$, it is apparent from equation 4 that f_c contributes to the dynamic stiffness of the system while f_s provides damping. The stops shown in Figure 1 suddenly contribute to the elements stiffness and significantly inhibits joint damping. As can be seen in Figure 7, the magnitude of f_s decreases with the amplitude right after the limit stops are hit.

To obtain the approximate solution, equations 3 and 5 are substituted into equation 1. After equating the linearly independent terms, the phase shift ψ is eliminated by using the relation $\sin^2\psi + \cos^2\psi = 1$. Then the following two nonlinear algebraic equations are obtained.

$$kB + f_b - f_1 = 0 = g_1(A, B, \omega) \tag{6}$$

$$[(k - m\omega^2)A + f_c]^2 + [\omega cA - f_s]^2 - f_o^2 = 0 = g_2(A, B, \omega) \tag{7}$$

Equations 6 and 7 are solved iteratively to get the frequency response of the vibratory amplitude A and the permanent offset B.

2.3. Calculation of Resonant Response

By holding the system parameters constant, the resonant vibratory amplitude A is obtained as

$$\frac{\partial A}{\partial \omega} = 0 \qquad \text{at} \quad \omega = \omega_m \tag{8}$$

To relate equation 8 with equations 6 and 7, it is observed that A and B are both functions of ω. Consequently, g_1 , g_2 are only functions of ω, and

$$\frac{dg_1}{d\omega} = \frac{\partial g_1}{\partial A}\frac{\partial A}{\partial \omega} + \frac{\partial g_1}{\partial B}\frac{\partial B}{\partial \omega} + \frac{\partial g_1}{\partial \omega} = 0 \tag{9}$$

$$\frac{dg_2}{d\omega} = \frac{\partial g_2}{\partial A}\frac{\partial A}{\partial \omega} + \frac{\partial g_2}{\partial B}\frac{\partial B}{\partial \omega} + \frac{\partial g_2}{\partial \omega} = 0 \tag{10}$$

From equation 6, we know $\partial g_1 / \partial \omega = 0$, thus equations 8 and 9 imply

$$\frac{\partial g_1}{\partial B}\frac{\partial B}{\partial \omega} = 0 \quad \text{and since from equation 6} \quad \frac{\partial g_1}{\partial B} = k \neq 0 \tag{11}$$

We have

$$\frac{\partial B}{\partial \omega} = 0 \qquad \text{at} \qquad \omega = \omega_m \tag{12}$$

Consequently, from equation 10

$$\frac{\partial g_2}{\partial \omega} = \{ c [\omega c A - f_s] - 2 m\omega [(k - \omega^2 m) A + f_c] \}(2A) = 0 \qquad \text{at} \quad \omega = \omega_m \tag{13}$$

Thus, the three equations that determine the resonant values A and B at the corresponding resonant frequency of excitation are

$$\begin{aligned} &g_1(A_m, B_m, \omega_m) = 0 \\ &g_2(A_m, B_m, \omega_m) = 0 \\ &\frac{\partial g_2}{\partial \omega}(A_m, B_m, \omega_m) = 0 \end{aligned} \tag{14}$$

To solve equation 14, it is noted that equation 6 is decoupled from equations 7 and 13. And from the relation (7) + (13)ω = 0, we have

$$F\omega_m^4 + G\omega_m^2 + H = 0 \tag{15}$$

where

$$F = 5(mA_m)^2$$

$$G = 3\{(c^2 - 2mk)A_m^2 - 2mA_m f_c\} \tag{16}$$

$$H = (kA_m)^2 + f_c^2 + 2kA_m f_c + f_s^2 - f_o^2$$

By substituting equation 13 into equation 7, we have

$$\{\omega_m cA_m - f_s\}^2\{1 + (\frac{c}{2m\omega_m})^2\} = f_o^2 \tag{17}$$

Therefore, from equations 14, 15, 16 and 17, the following iterative equations for calculating the resonant response can be obtained

$$B_m = \frac{f_1 - f_b}{k}$$

$$A_m = \{f_s + |f_o| / \sqrt{1 + (c/2m\omega_m)^2}\} / c\omega_m \tag{18}$$

$$\omega_m = \{(\frac{1}{2F})(-G + \sqrt{G^2 - 4FH})\}^{1/2}$$

To solve equation 18, group values of (A_m, B_m, ω_m) are first initialized to calculate the Fourier coefficients f_b, f_s, f_c. Iterations are then made utilizing equation 18 until A_m , B_m, and ω_m converge.

2.4. Calculation of Vertical Jumps

When the system parameters are constant, the vertical jumps occur when

$$\frac{\partial A}{\partial \omega} \to \infty \quad \text{or} \quad \frac{\partial \omega}{\partial A} = 0 \quad \text{at} \quad \omega = \omega_j \tag{19}$$

The above constraint is imposed on equation 7 to get the following relation as

$$\frac{dg_2}{dA} = \frac{\partial g_2}{\partial \omega}\frac{\partial \omega}{\partial A} + \frac{\partial g_2}{\partial A} = \frac{\partial g_2}{\partial A} = 0 \qquad \text{at} \quad \omega = \omega_j$$

where

$$\frac{\partial g_2}{\partial A} = [(k - m\omega^2)A + f_c](k - m\omega^2 + \frac{\partial f_c}{\partial A})$$

$$+ (\omega cA - f_s)(\omega c - \frac{\partial f_s}{\partial A}) = 0 \qquad \text{at} \quad \omega = \omega_j \tag{20}$$

From the relation $(A\partial f_s/\partial A + f_s)(20) - (2Af_s)(7) = 0$, we obtain the following equation

$$R\omega^4 + S\omega^2 + T = 0 \tag{21}$$

where

$$\begin{aligned}
R &= \left(A\frac{\partial f_s}{\partial A} - f_s\right)(mA)^2 \\
S &= \left\{(c^2-2mk)\left(A\frac{\partial f_s}{\partial A} - f_s\right) + (2m)\left(f_s\frac{\partial f_c}{\partial A} - f_c\frac{\partial f_s}{\partial A}\right)\right\} A^2 \\
T &= \left\{\left(Ak - 2f_c\right)\frac{\partial f_s}{\partial A} - \left(k + 2\frac{\partial f_c}{\partial A}\right) f_s\right\}(k A^2) - (2Af_s)\left(f_c\frac{\partial f_c}{\partial A} + f_s\frac{\partial f_s}{\partial A}\right) \\
&\quad + \left(f_s^2 + f_c^2 - f_o^2\right)\left(f_s + A\frac{\partial f_s}{\partial A}\right)
\end{aligned} \tag{22}$$

and the frequencies at which jumps occur are obtained by

$$\omega_j = \left\{\left(-S \pm \sqrt{S^2 - 4RT}\right) / 2R\right\}^{1/2} \tag{23}$$

Analogous to the approach used in the last section, equation 23 together with equations 6 and 7 provide the basis for calculation of the vertical jumps.

3. NUMERICAL RESULTS

The numerical results are presented in this section. Part 1 shows representative plots of the amplitude as a function of frequency of excitation and discusses how various parameters affect the response. Part 2 indicates how changes in the system parameters affect the peak response amplitude. The effects of gap length on dynamic response are shown in Part 3 and Part 4. Part 3 describes the existance of disconnected amplitude solutions and how the gap and static preload affect them. Part 4 introduces the minimum gap length for unstable response to appear and how instability is affected by preload. Finally, two cases of transient response are given in Part 4. They show that the system parameters that dictate the steady-state behavior of the system also control transient response.

3.1. Frequency Response

To examine the validity of the approximate method; equation (1) is solved directly using the Runge-Kutta method. The steady-state response is then obtained from the "long time" transient solution. The results are compared with the ones calculated by the approximate method. These comparisons are plotted in Figures 8-12 in which the discrete symbols denote the transient solutions. These figures show that a good agreement exists between the two approaches.

In Figure 8, the influence of gap length δ on the vibratory amplitude frequency response is shown. For $\delta=0$, the system is linear. For $\delta \to \infty$, the friction joint is dominated by friction damping, and the system behaves plastically. In between, a transition region exists for a certain range of δ values where the system shifts from elastic to plastic behavior. In this region, the vibratory amplitude A may become multi-valued at some fixed excitation frequencies. This phenomenon is typically referred to as "unstable response". A typical case for $\delta=20$ is shown in the figure.

Unstable response can also be seen in Figure 9, in which the amplitude is calculated for several different values of the normal load μN. For $\mu N = 2.0$, the system response is stable (vibratory amplitude is single valued). Unstable behavior is clearly seen in cases of $\mu N = 1.0$ and 1.5. For $\mu N = 1.5$, the vibratory amplitude has two disconnected response curves. For $\mu N = 1.0$, the response curve becomes connected, even though point jumps remain at frequencies between 1.035 and 1.04. This implies that for even lower μN values, the system response will become stable again. The physical explanation of this behavior is that at low μN values, the friction damping has little effect on the system response which is primarily dominated by the constant stiffness k and viscous damping c, and consequently, the system behaves linearly. For high μN values, the friction element is partially stuck due to the stronger friction resistance. Under this condition, neither of the limit stops is hit during the motion cycle. As a result the energy dissipation per cycle monotonously increases with amplitude, and the system response is stable. For normal loads in the median range, as the cases of $\mu N = 1.5$ and 1.0 shown in the figure, the limit stops are hit by the element during the motion cycle. The system response becomes meta-stable or unstable. This is due to the fact that the energy dissipated by friction per cycle

remains constant while, because of the limit stops, the element stiffness significantly increases with amplitude. This results in the multi-valued response indicated in Figure 9.

Multi-valued behavior is also seen in Figure 10; where the amplitude is calculated for various stiffness ratios k_d / k. A region of unstable behavior is seen for $k_d / k = 0.25$, where a disconnected closed curve occurs. The appearance of disconnected regions in the more general system model analyzed here agrees well with those observed in Iwan's [1] work.

The effect of static load f_1 on the vibratory amplitude frequency response is shown in Figures 11 and 12. The static load causes a permanent offset represented by the symbol B, as indicated in equation 3. When the system is excited by a large excitation force f_o at the resonant frequency, both limit stops (shown in Figure 1) are hit during the motion cycle, and the offset has little effect on the vibratory amplitude. However, at some off-resonant frequencies, the response is sufficiently low that there is a difference in the response since without the static preload the limit stops would not be encountered during the motion cycle. However, once the static load is applied, the permanent offset thus generated adds to the dynamic displacement and causes the friction element to hit one of the stops and reduces damping in the system. Consequently, the vibratory amplitude increases at off resonant frequencies as illustrated in the figure.

Based on the above argument, it is then understandable that the static load may even raise the maximum amplitude of the system under low excitation force f_o. This fact is depicted in Figure 12 where the maximum amplitude is increased when the static load $f_1 = 10$.

Thus, it is seen that under certain conditions static preload can have a significant effect on vibratory response. For some excitation, the presence of a large static load may even eliminate the multi-valued response and stabilize the system. This means that gravitational effects may strongly affect the dynamic response of structures that are ground tested and it might be quite different from the actual response that would occur in space. Therefore, this effect needs to be carefully analyzed in order to properly interpret laboratory test data so as to predict the response of the full-scale structure in space.

3.2. Peak Amplitude Response[1]

First consider the system's response when there are no stops to limit slip in the nonlinear element. The amplitude of peak response will then depend on how stiff the nonlinear spring k_d (relative to the system's stiffness, k) and the value of the slip load, μN. Representative results are presented in Figure 13. For sufficiently large μN, the friction element is stuck and the system is linear. The system also behaves linearly when μN is zero since no energy is dissipated by friction. It can be seen from the plot that the friction damping effect is only significant for μN between 0 and some maximum value, μN_{max}. Furthermore, a minimum peak vibratory amplitude exists for a certain μN value, as shown in the figure. This fact has been discovered and experimentally verified by Griffin [3].

Figure 14 shows the plot of resonant frequency vs. normal load μN at gap length $\delta = \infty$. It is observed that resonant frequency increases with the normal load, and hits a maximum when the normal load is sufficiently large that the friction element is always stuck. Again this indicates that the effect of normal load is only significant over a finite range.

The effect of gap length on the peak vibratory amplitude response is indicated by the results depicted in Figure 15. A plot of the resonant frequency vs. gap length is given in Figure 16. In both figures, the γ in the abscissa denotes the nondimensional gap length introduced in equation 43. In both plots it can be seen that for constant normal load μN, a transition region exists in which the gap length strongly affects the dynamic response. For gaps larger than a certain value, the limit stops shown in Figure 1 will no longer limit slip in the friction element and, consequently, further increases in gap length will not affect the peak response. It is clear that the gap length effect is only significant in the transition region. This is depicted in Figures 17 and 18, which are the scaled versions of the Figures 15 and 16. The critical gap length δ_{cr} is defined as the value beyond which the peak response is unchanged. This value which will be investigated in the next section is used as the scale length in the abscissa for both plots.

---

[1] Since in an unstable response condition the system may have several resonant amplitudes, here to avoid ambiguity, "peak amplitude" refers to the maximum resonant amplitude.

At $\delta=0$ the system peak response is dominated by stiffness and viscous damping. At $\delta=\infty$, the system peak response depends on the stiffness, and both viscous and friction damping. The difference between the two amplitudes and frequencies are used to scale the ordinates in Figures 17 and 18 respectively.

Since the peak response is only affected by the normal load $\mu N = 0$ to μN_{max}, the results for different normal loads all lie fairly closely together in a band as indicated in Figure 17 for amplitude and Figure 18 for frequency. It was shown in Figure 13, that the lowest peak response comes at a specific μN value (0.1 for the system considered here) and this case provides a lower bound on the response when the data is depicted as in Figure 17. The normal loads which are greater or less than this value then approach this common lower bound of the band.

As the normal load goes to zero or when it approaches μN_{max} the system becomes linear and the stiffness has no effect on the lower bound curve of the band. However, an increase in the nonlinear element's stiffness k_d/k can affect the upper bound of the curves. This is shown in Figures 19 and 20 for peak amplitude and frequency respectively.

3.3. The Effect of Critical Gap Length on Unstable Response

The phenomenon of disconnected amplitude solutions is examined in this section by considering the equations for maximum response. First, equation 17 is rearranged into the following form.

$$-f_s(A,B) = |f_o| / \sqrt{1. + (c/2m\omega_m)^2} \quad - \omega_m cA = g_s(A,B,\omega_m) \tag{24}$$

The offset B can be calculated from the first equation in 18 as a function of A and then ω_m from the last equation in 18. Therefore, conceptually, functions g_s and f_s are dependent on the amplitude A only. Thus, these functions can be presented in a plot with amplitude A as the common abscissa. These are shown in Figures 21 and 22 for a range of values of f_o and f_1 respectively. In the plots, the intersections indicate the resonant amplitudes.

As can be seen, the function g_s is almost a linear function of A due to the fact that the

resonant frequency is nearly constant (approximately 1.0). In Figure 21, it is clear that for different excitation levels, an unstable region of two disconnected amplitude response curves exists between points c1 and c2. This is indicated by the three resonant amplitudes shown in the figure: the upper two values are the maximum and minimum amplitudes of the upper closed response curve, while the lowest one is the maximum amplitude of the lower response curve. Physically, point c1 indicates the maximum excitation for which the stable response is obtained. In this situation, both of the limit stops shown in Figure 1 are not encountered by the friction element during the motion cycle. This indicates that for constant excitation f_o, a critical gap length δ_{cr} exists beyond which the response remains unchanged. This critical value can be obtained by the geometric requirement at point c1 that the slopes of the curves as well as their values are equal, i.e.

$$\frac{\partial f_s}{\partial A} = -\frac{\partial g_s}{\partial A} = \omega c \qquad \text{and} \qquad -f_s = g_s \ , \qquad \text{when } B \text{ is constant} \tag{25}$$

Point c2 indicates the maximum excitation for disconnected solutions to appear. Alternatively, for constant excitation f_o, this point indicates the maximum gap length δ_m for which the system has disconnected amplitude solutions. It is clear from the figure that in the disconnected amplitude response region, an upper response curve exists (indicated by the upper two resonant amplitudes) when the friction element hits the stops during the motion cycle, while a lower response curve exists (indicated by the lower resonant amplitude) when it does not reach at least one of the stops. Since the lower response curve is not affected by the gap (stops are not hit), the lower resonant amplitude is the same for gap lengths larger than or equal to δ_m at a constant excitation f_o. As can be seen in the figure, point c2 is where the friction element touches both of the stops at the lower resonant amplitude. Therefore, the gap length δ_m can be determined from the equation below

$$\delta_m = 2\left(A_\infty - \frac{\mu N}{k_d}\right)$$

where A_∞ = the resonant amplitude at $\delta = \infty$ (26)

In the above, the A_∞ is used since the lower resonant amplitude is the same for gap length larger than or equal to δ_m.

The effect of static preload on the region where the disconnected solutions occur is depicted in Figure 22. It is apparent that the static load tends to play an on/off role on this region. When this load is below a certain value, only the lowest resonant amplitude is affected and the response remains disconnected. Once this load is raised above a critical value (20 in the case shown), the amplitude solutions become single valued.

3.4. Minimum Gap Length for Vertical Jumps

As was discussed in the last section, disconnected solutions exist between limit gaps δ_{cr} and δ_m for constant excitation f_o. For gap length less than δ_m, the system response becomes connected; however, discrete point jumps remain. Thus, unstable response can occur until the gap length is further reduced below a limit δ_j.

The reponse depicted in Figure 23 may be used to illustrate this argument. The locus of vertical jumps is presented in broken lines which define a closed region. In this plot, the excitation f_o is varied while the gap is kept constant. The intersections of the response curves and the jump locus indicate where individual point jumps occur. In the figure, it is clear that vertical jumps only occur when the limit stops shown in Figure 1 are hit during the motion cycle. The jumps disappear when the excitation f_o is large enough that the response curve passes beyond point a_1 or a_2 (whichever is passed by secondly). At constant excitation, the limit gap δ_j for vertical jump can be obtained when the response curve intersects the jump locus at either point a_1 or a_2 (whichever leads to the smaller δ_j). The choice between points a_1 and a_2 as the passing point is affected by the stiffness k_d / k. When the stiffness $k_d / k \to \infty$, the response curve is more slanted to the left and point a_2 will be passed by first in decreasing gap length at constant excitation. The point a_1 is then the intersection used to determine the limit gap δ_j, and vice versa.

In Figure 24, the effect of static preload on the jump locus is depicted. It is seen that the closed region of the jump locus is shrinked as the load is increased. At the same time, the jump limit gap δ_j is raised in value.

The limit gaps δ_{cr}, δ_m, δ_j as functions of the normal load μN are shown in Figure 25.

As shown in the plot, three regions exist. When the normal load μN approachs zero, regions II and III shrink, and all the limit gaps δ_{cr}, δ_{m}, δ_{j} tend to infinity. The system response then becomes linear.

At a large value of μN, limit gap curves δ_{cr} and δ_{m} superpose on each other, and the disconnected response (region II) disapears. However, the discrete jumps (region III) remain. This remains the case until μN reaches μN_{max}, after which the friction element becomes stuck and the gap no longer affects response. As can be implied from the figure, the limit gap curves δ_{cr}, δ_{m} then descend to merge with δ_{j} at one point.

3.5. The Effects on the Transient Solutions

One reason for studying the system's steady-state is to gain a better understanding of its transient response. We have been examining conditions under which the steady-state response is unstable. These conditions also affect transient response. For example, when the system parameters are such that its response tends to be unstable then slightly altering one of the parameters can lead to quite different transient response.

Figures 26 and 27 indicate how the gap affects the transient response. Figure 26 shows the initial response of the system while Figure 27 shows how the vibratory amplitude changes over a large period of time. Two cases are plotted in each figure, one corresponding to $\delta=23$ and the other to $\delta=30$. For short times (Figure 26), responses are identical. However, for longer times they differ radically. It is known from the previous sections that for conditions corresponding to unstable response, different initial conditions may lead to different vibratory amplitude at the steady-state. In the previous section, we showed that the gap length also affects the unstable response. Consequently, even for the same initial conditions, changes in the gap length can lead to quite different transient responses.

The effect of static preload is illustrated in Figures 28 and 29. Again, Figure 28 shows the plots of the displacement for short times, and Figure 29 shows the long time response. In this particular case, the load accentuates the response for short times, and attentuates it later.

In regard to the ground testing on a sub-scaled model of a large space structure, the above plots indicate an important result. The examples shown in Figures 27 and 29 imply that a larger gap may reduce the amplitude of response while the applied static load may contribute an opposite effect. Compared to the full-scale structure, the sub-scaled model tends to have larger joint tolerances relative to its smaller overall size. In addition, a large static preload (from gravity) may be present during ground testing. Since these two factors sometimes contribute opposite effects, they have an unknown qualitative and quantitative effect on the test results. This indicates the need for a careful analysis of the experiment data in order to predict properly the response of the full-scale structure in space.

4. CONCLUSION

The approximate solution method based on a describing function approach has been verified to be an effective tool in studying the response of systems containing a friction joint with limited slip. It is believed that this approach could be extended to investigate the steady-state response of a large truss-like jointed structure and could provide a basis to calculate transient response.

It has been found that under certain conditions the vibratory amplitude of the system may become multi-valued at certain excitation frequencies. A large jointed structure may have significant variations in the joint properties from joint to joint due to machining differences. As a result some of the joints may experience the conditions that lead to multi-value response. Consequently, it may be difficult to get repeatable experimental results since the structure may settle into different patterns of response depending on fairly subtle aspects of how the loads are applied. The difficulty is intensified for laboratory tests of sub-scaled models of space structures since the scatter in the joint's free-play is relatively larger (with respect to the smaller dimensions of the model joint).

This work also shows that in some circumstances, the presence of static preloads may affect significantly the system's dynamic response. In this case if a large structure is ground tested it may be necessary to first correlate the data with an analytical model of the structure that includes preload effects. Then eliminate the preloads in the model and predict its behavior in space.

Lastly, a way of looking at system response in terms of non-dimensionalized joint properties has been developed. These curves are useful because they indicate how sensitive a system is to changes in joint tolerances. When one makes a scale-model of a joint the relative tolerances and free-play in the joint increase. The computed results indicate an approach for assessing system sensitivity to such changes.

5. FIGURES

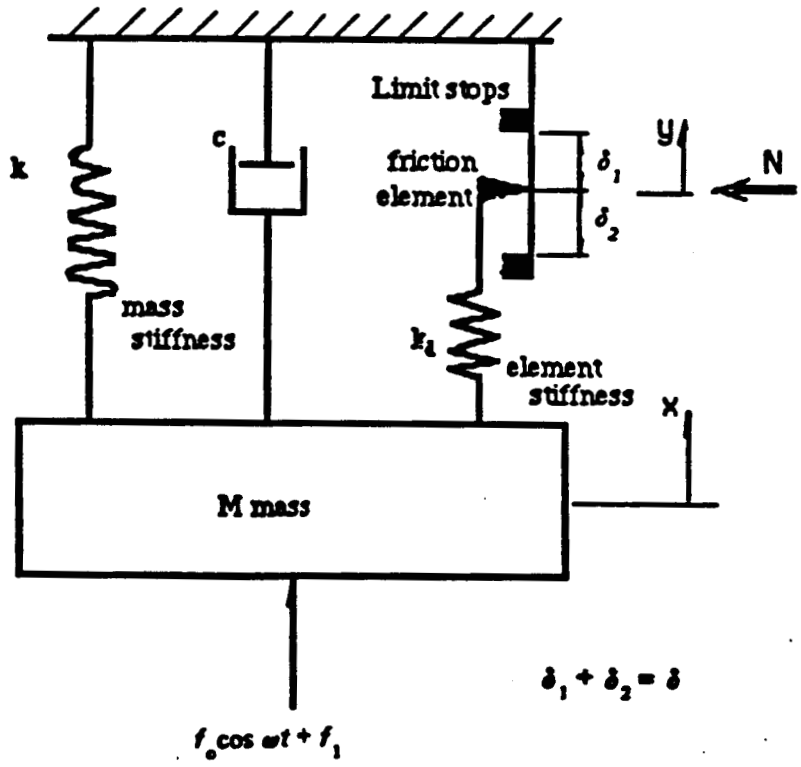

Figure 1: Single Degree of Freedom System with a Limit Slip Joint

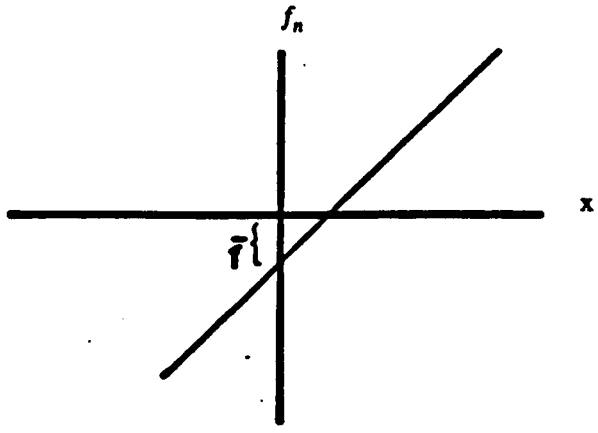

Figure 2: Non Slip

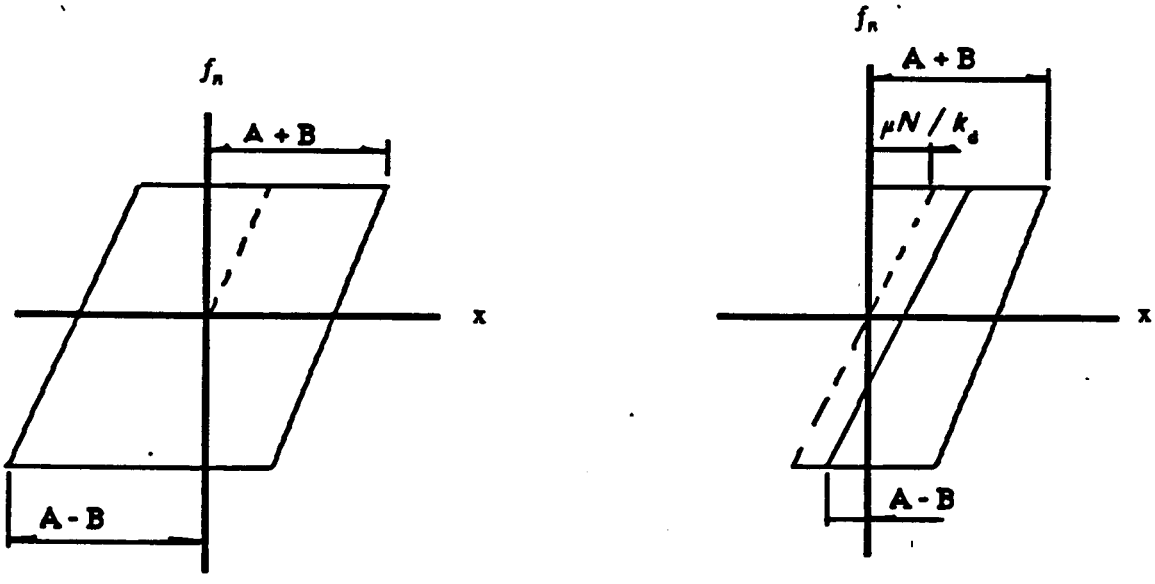

Figure 3: Pure Slip

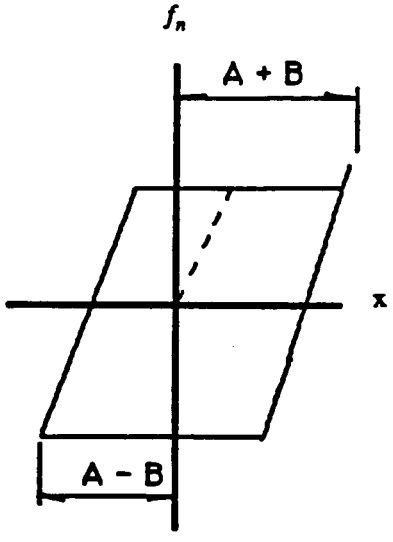

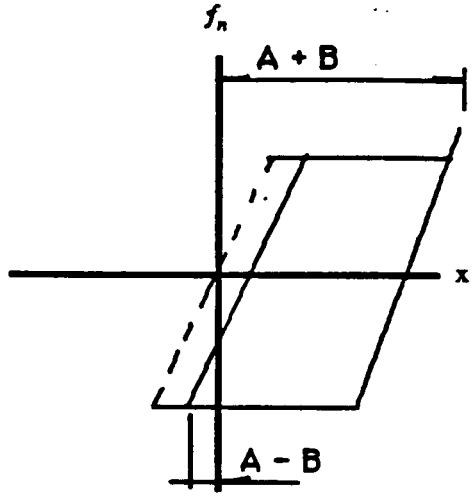

Figure 4: Slip with Upper Limit

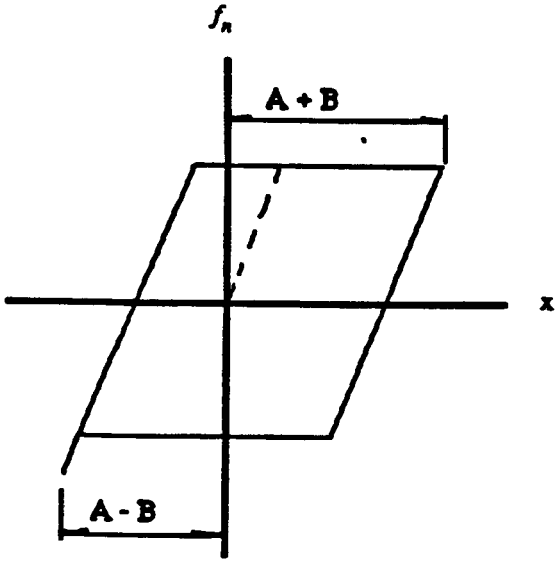

Figure 5: Slip with Lower Limit

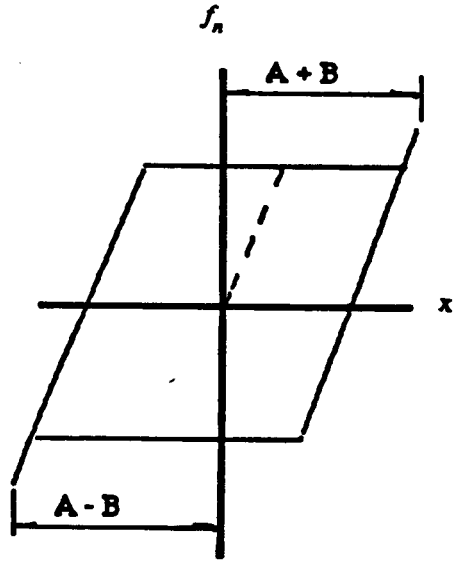

Figure 6: Slip with both Limits

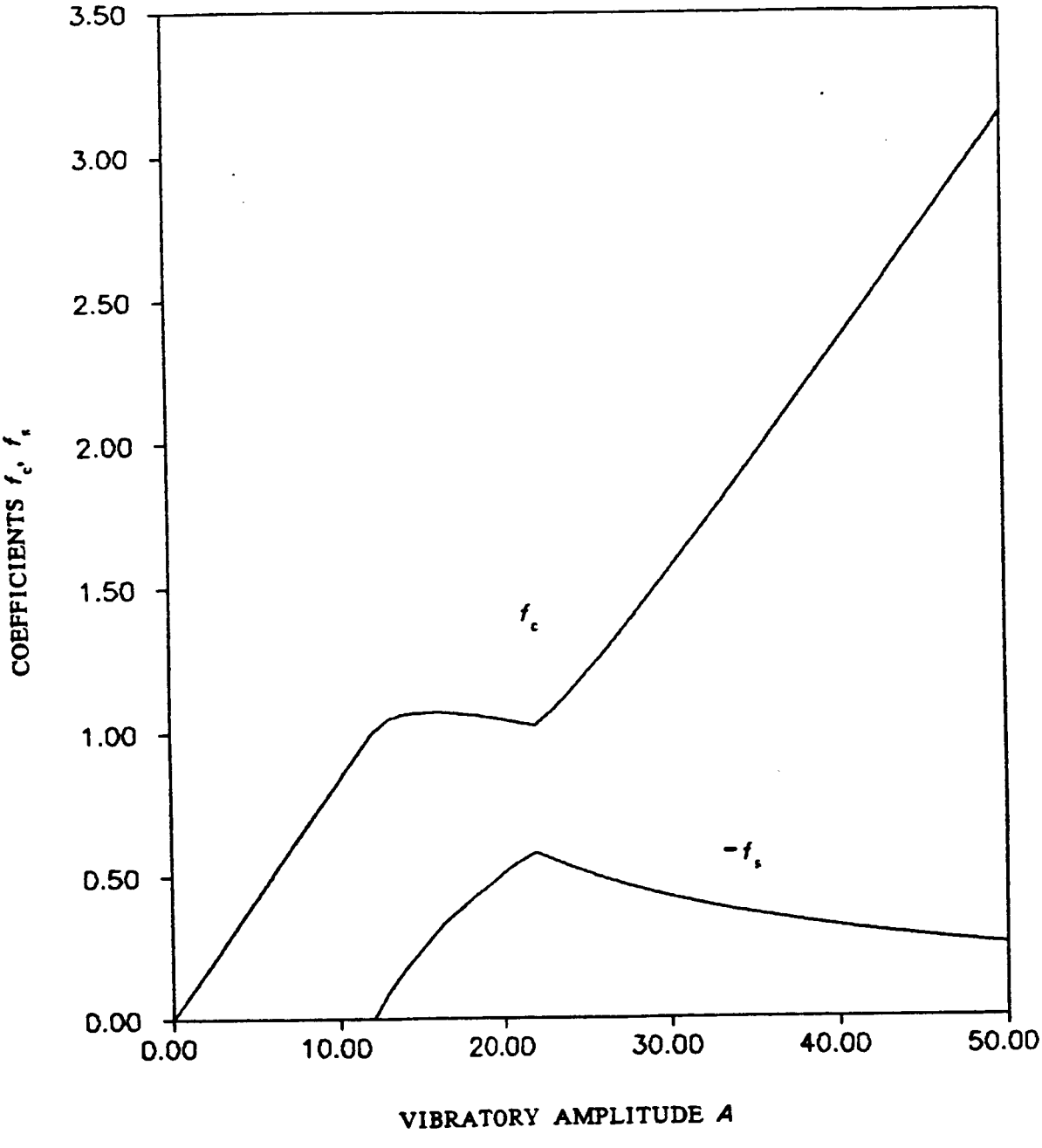

Figure 7: Fourier Coefficients f_s, f_c vs. Vibratory Amplitude A , δ=20

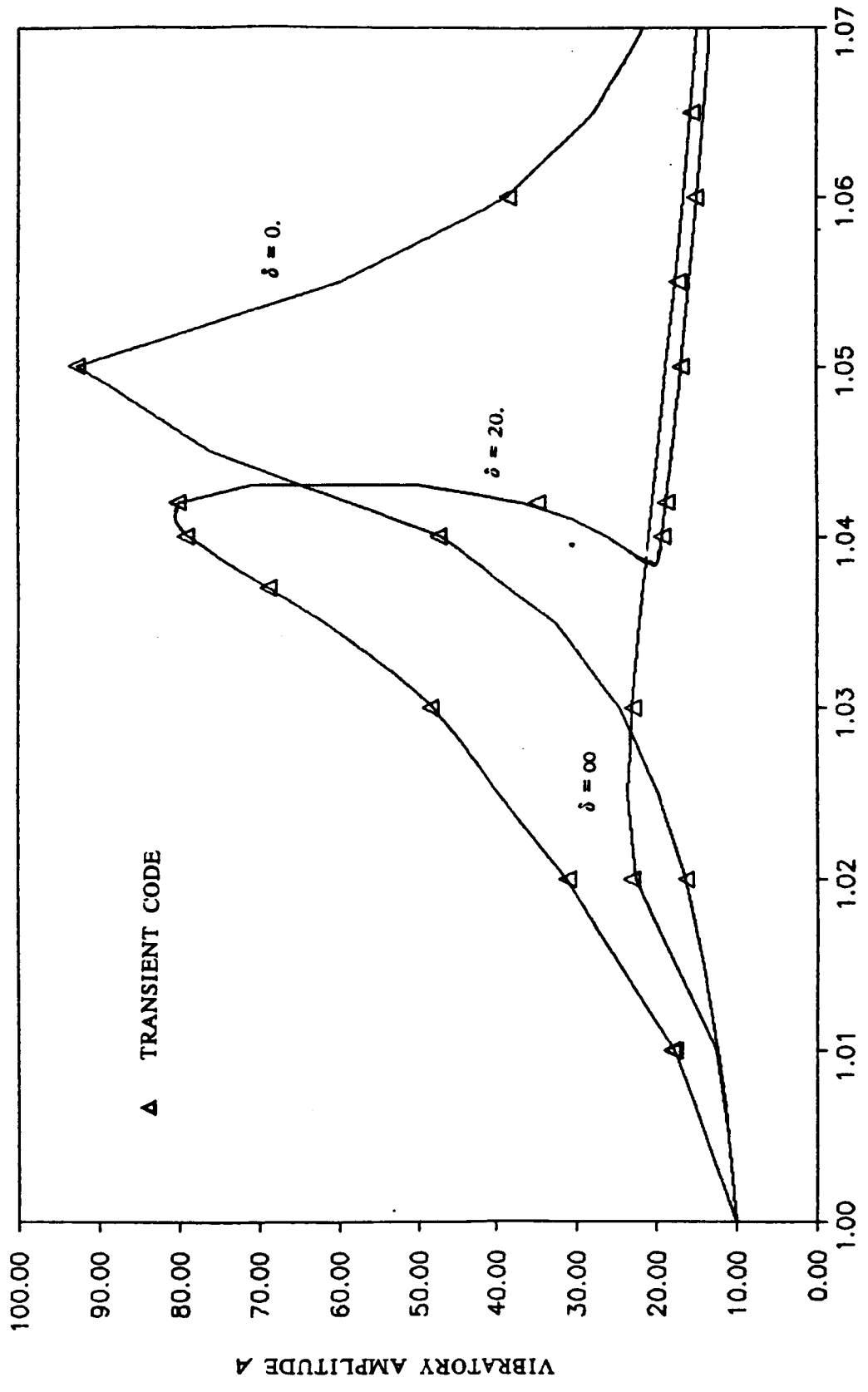

Figure 8: Vibratory Amplitude vs. Frequency with Varied Gap Length δ, f_o=1, f_1=0, m=1,c =0.01, k_d / k = 0.1,μN = 1.0, q = 0.5

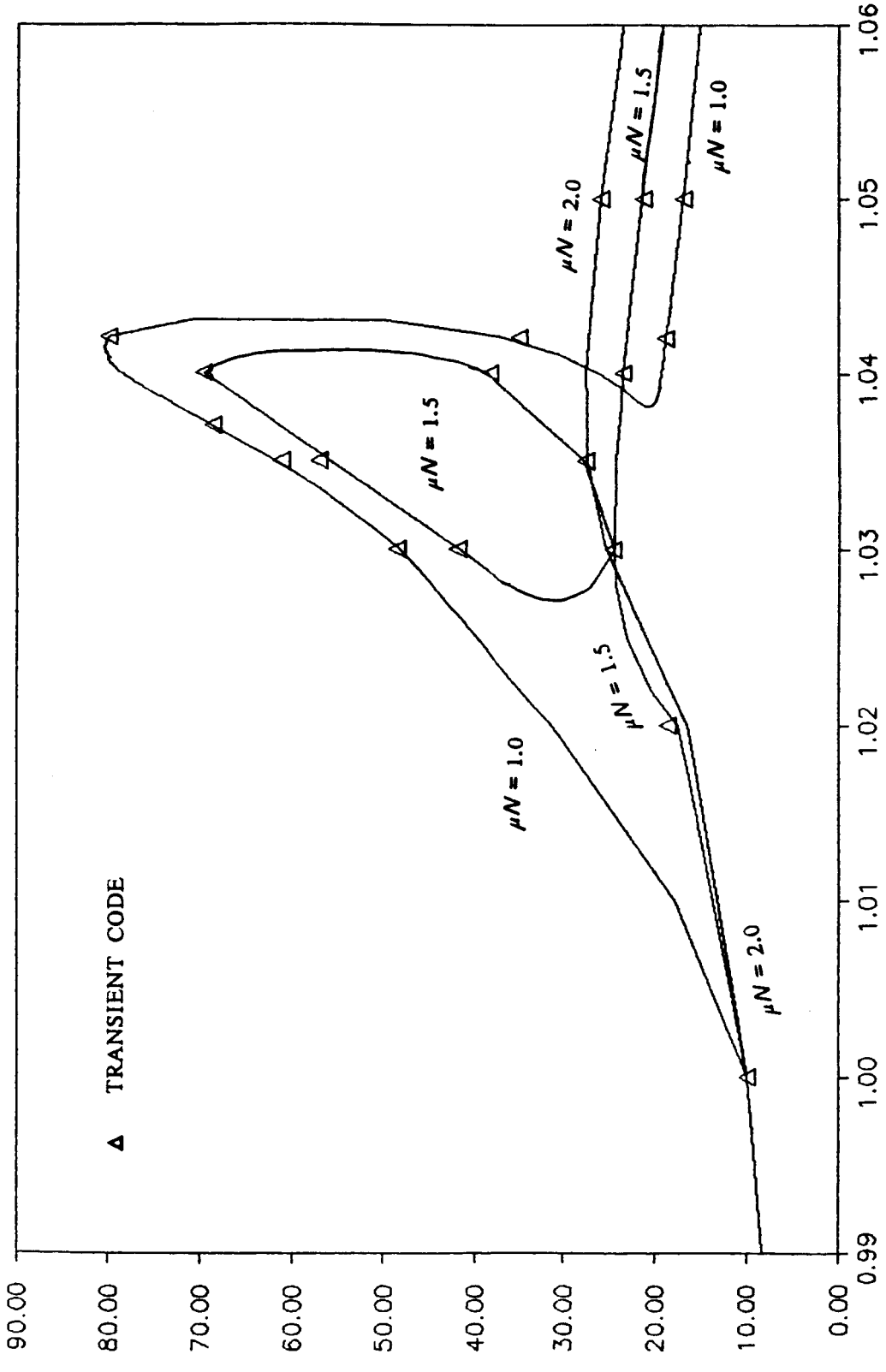

Figure 9: Vibratory Amplitude vs. Frequency with Varied Normal Load μN, f_o=1.0, f_1=0, m = 1, c = 0.01, k_d/k = 0.1, δ=20, q=0.5

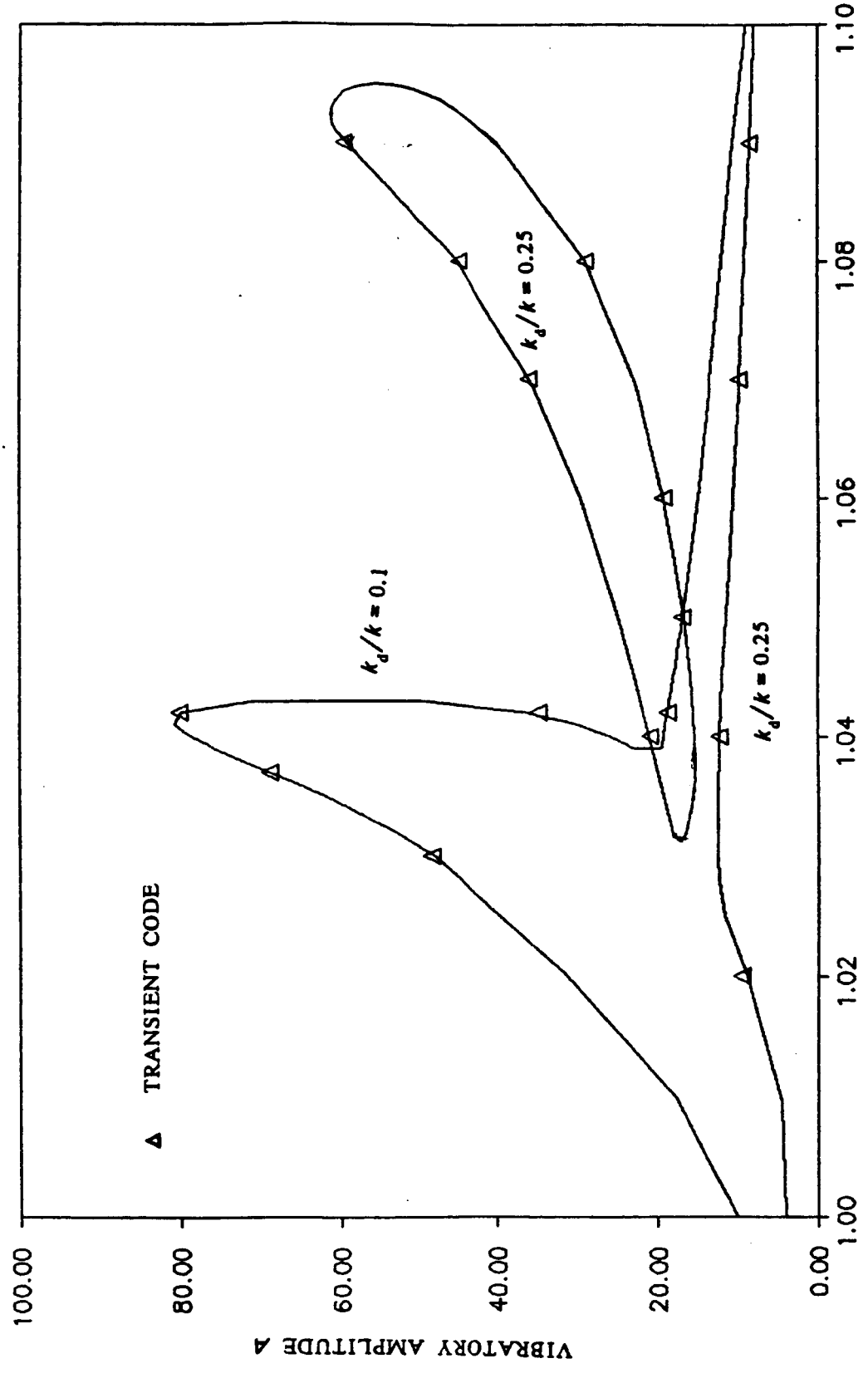

Figure 10: Vibratory Amplitude vs. Frequency with Varied Stiffness k_d/k, f_0=1.0, f_1=0, m = 1, c = 0.01, μN=1.0, δ=20, q = 0.5

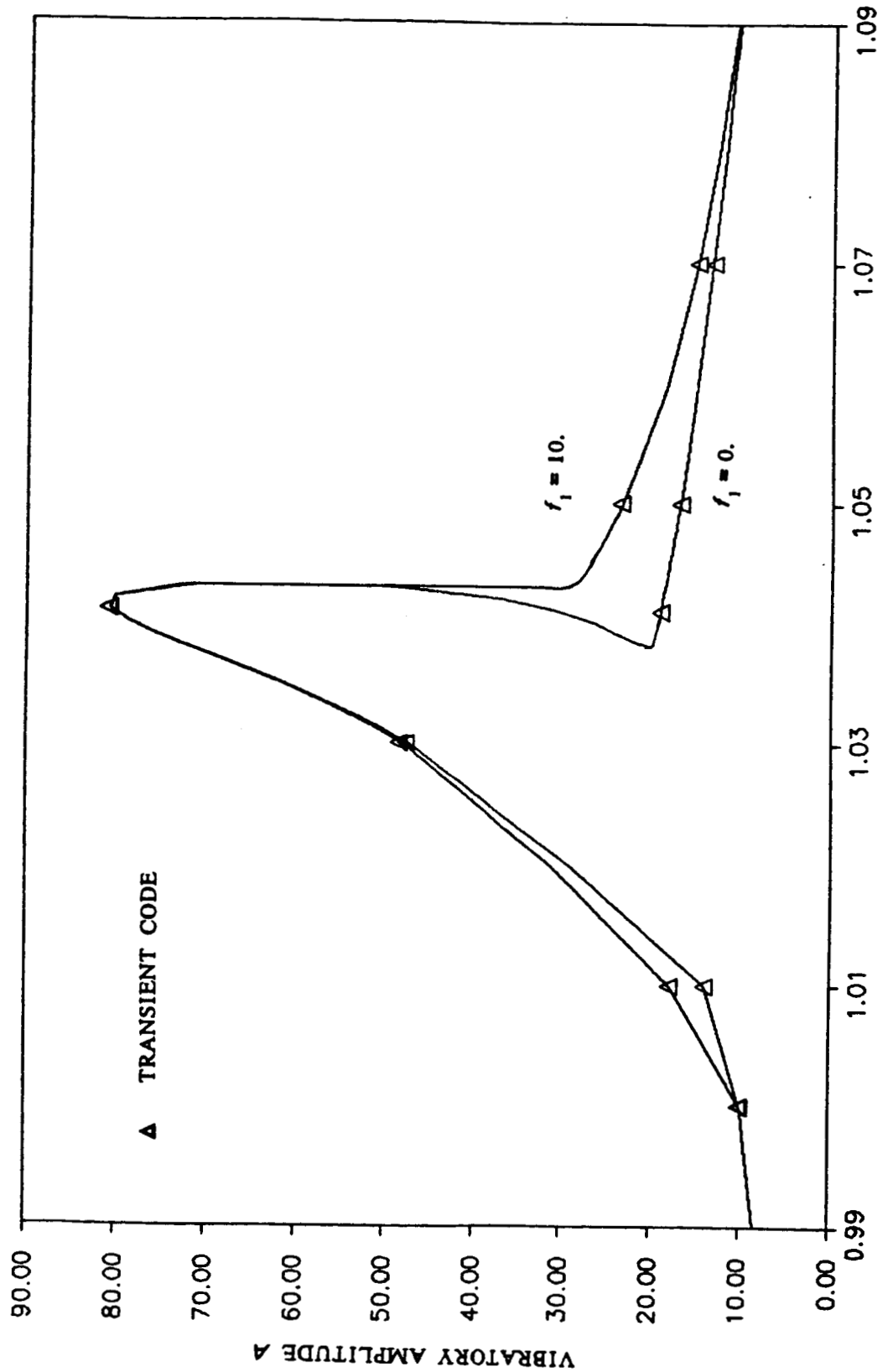

Figure 11: Static Load on Amplitude Frequency Response Under High Excitation, f_0=1, m=1, c=0.01, k_d/k=0.01, μN=1.0. δ=20, q = 0.5

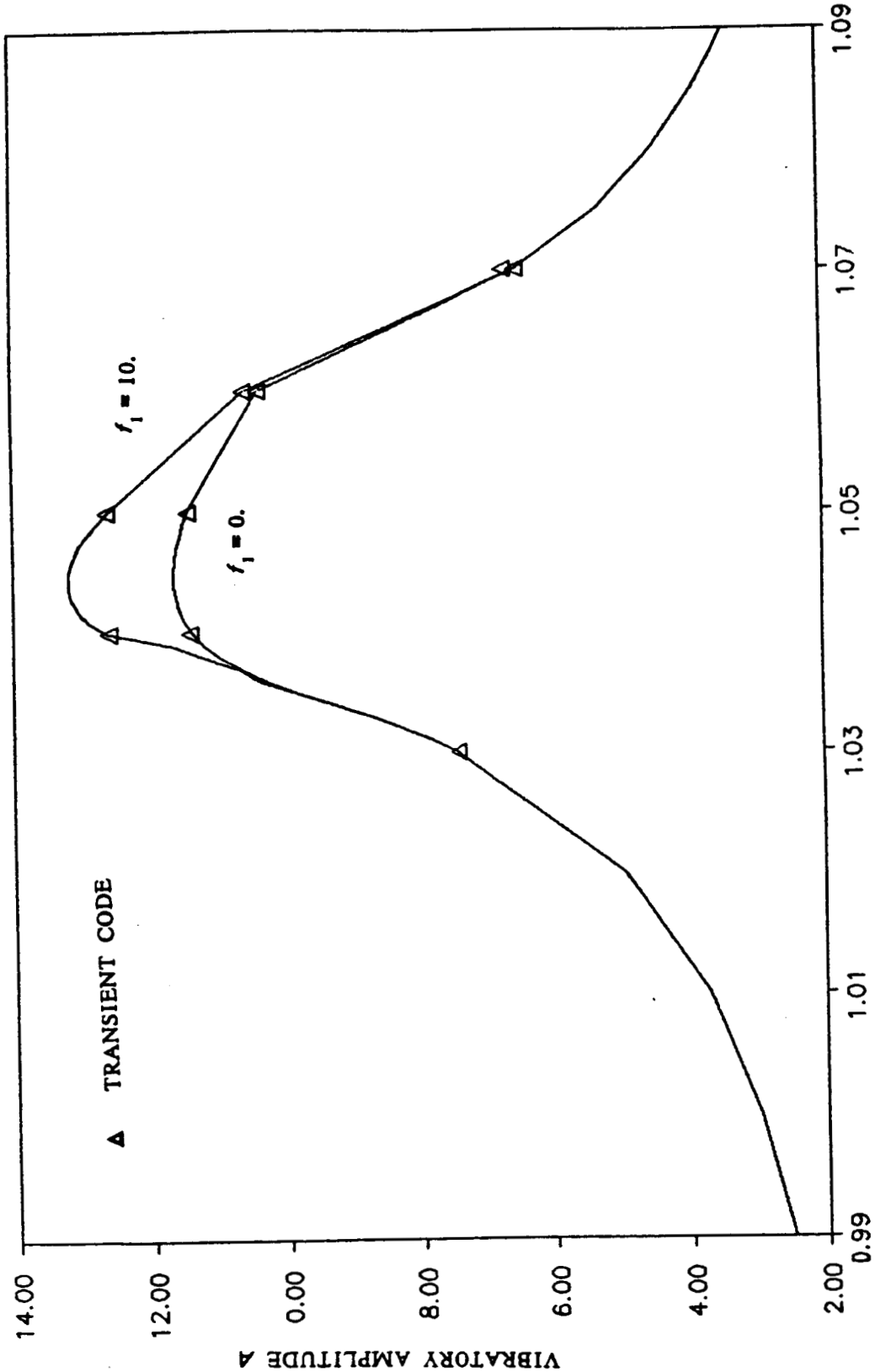

Figure 12: Static Load on Amplitude Frequency Response Under Low Excitation, f_0=0.3, m=1, c=0.01, k_d/k=0.01, μN=1.0, δ=20, q = 0.5

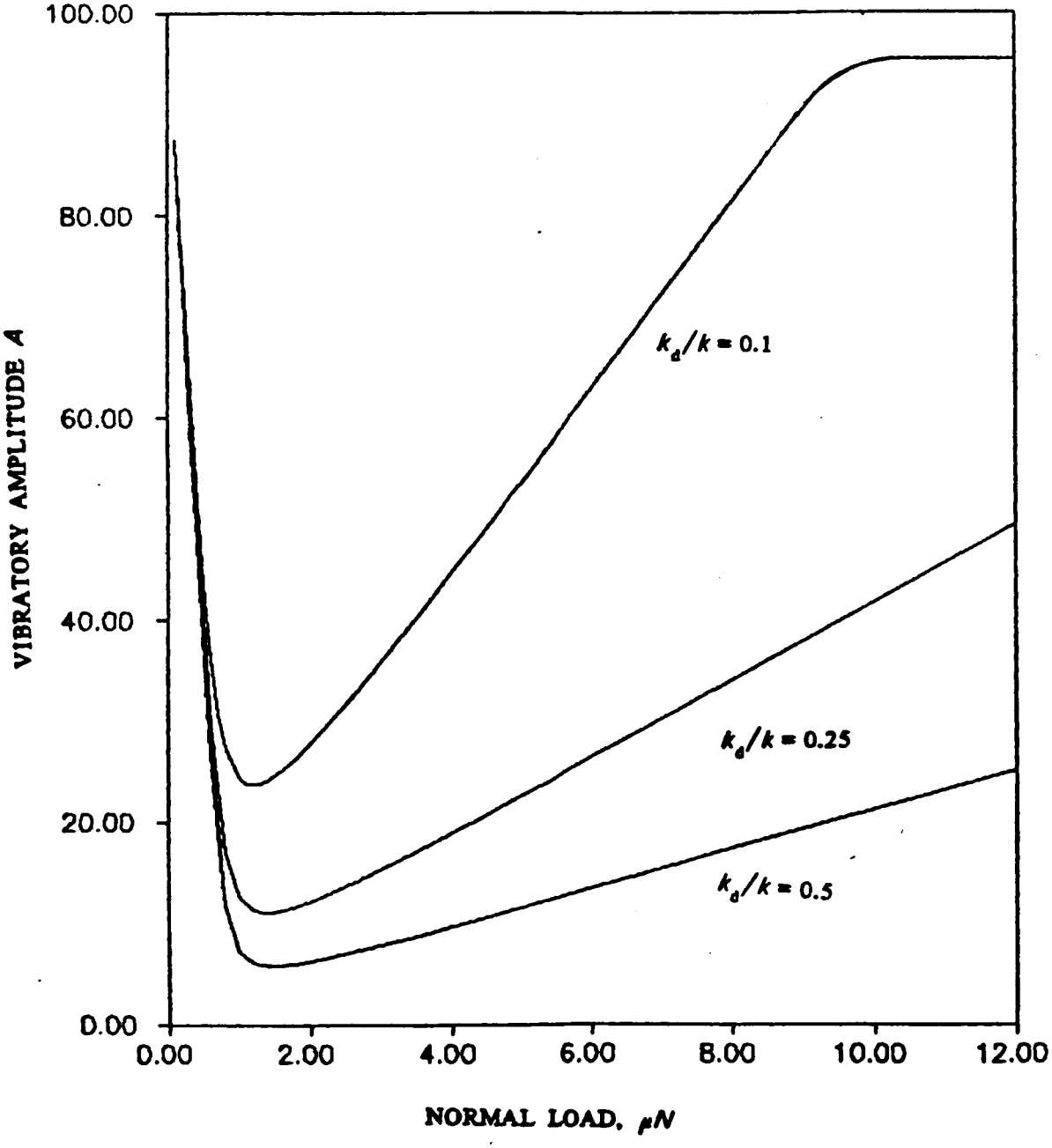

Figure 13: Max. Vibratory Ampiltude vs. Normal Load μN when Gap Length $\delta = \infty$, $q = 0.5$

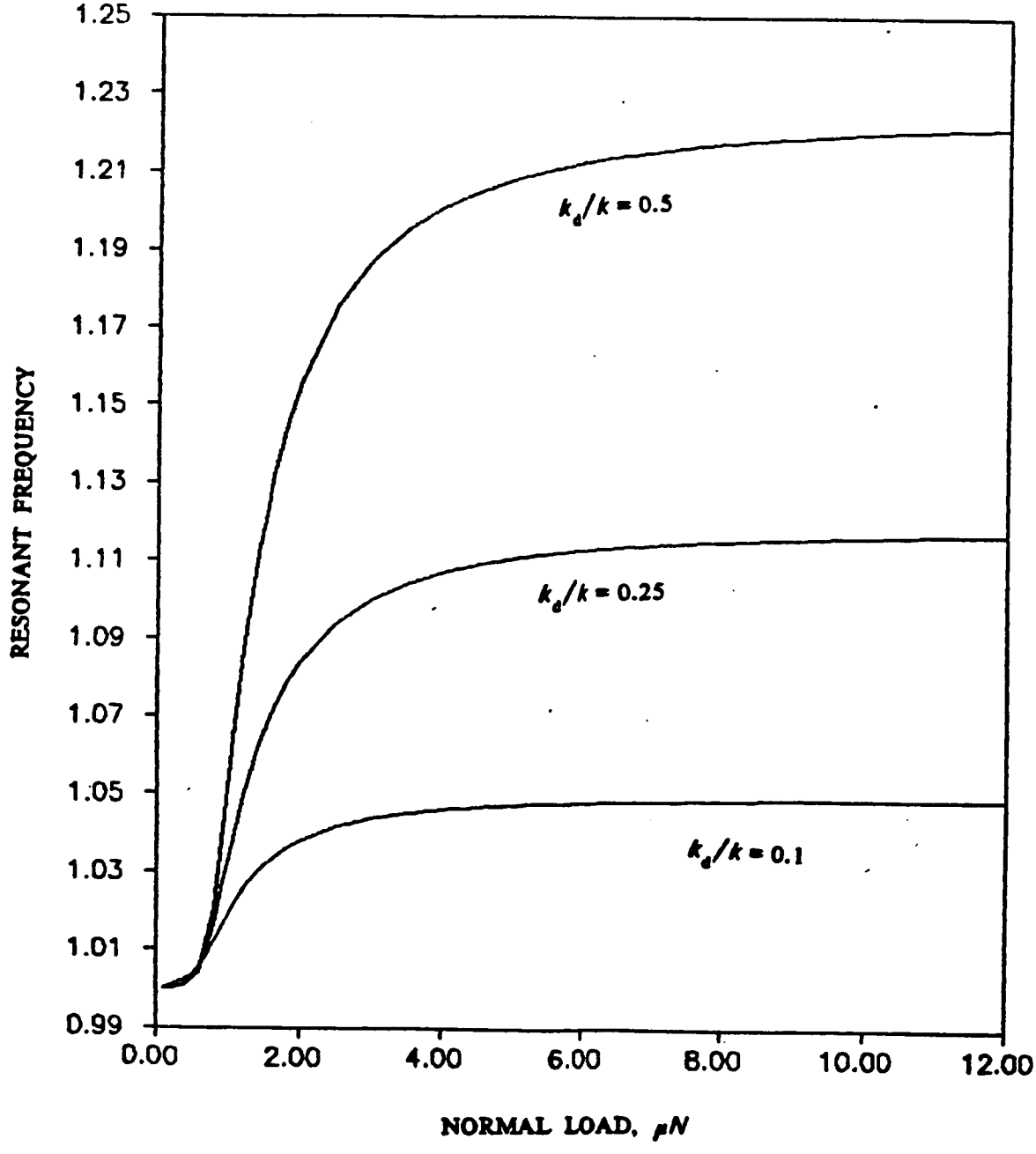

Figure 14: Resonant Frequency vs. Normal Load μN when Gap Length $\delta = \infty$, $q = 0.5$

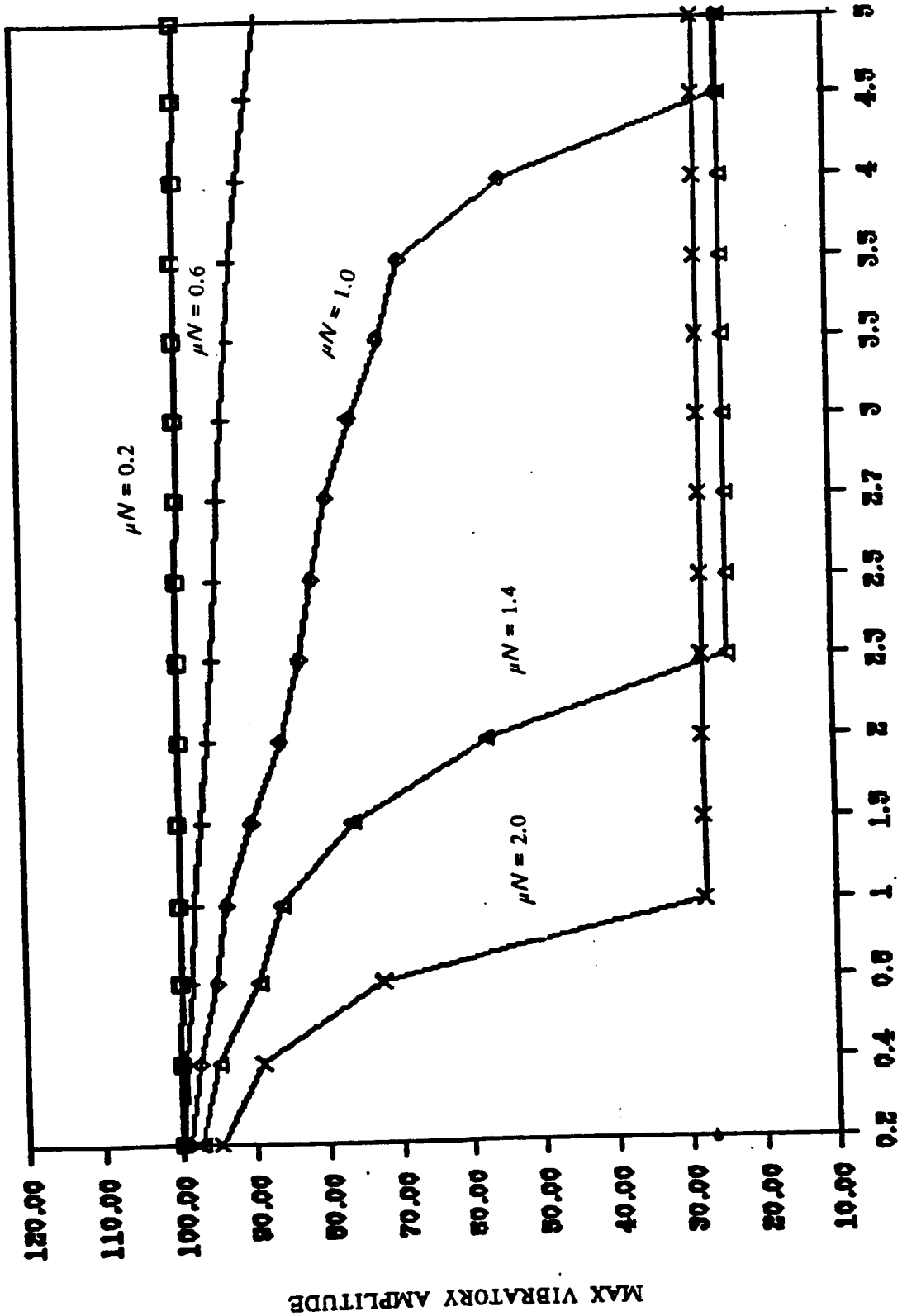

Figure 15: Max. Vibratory Amplitude vs. γ , $q = 0.5$

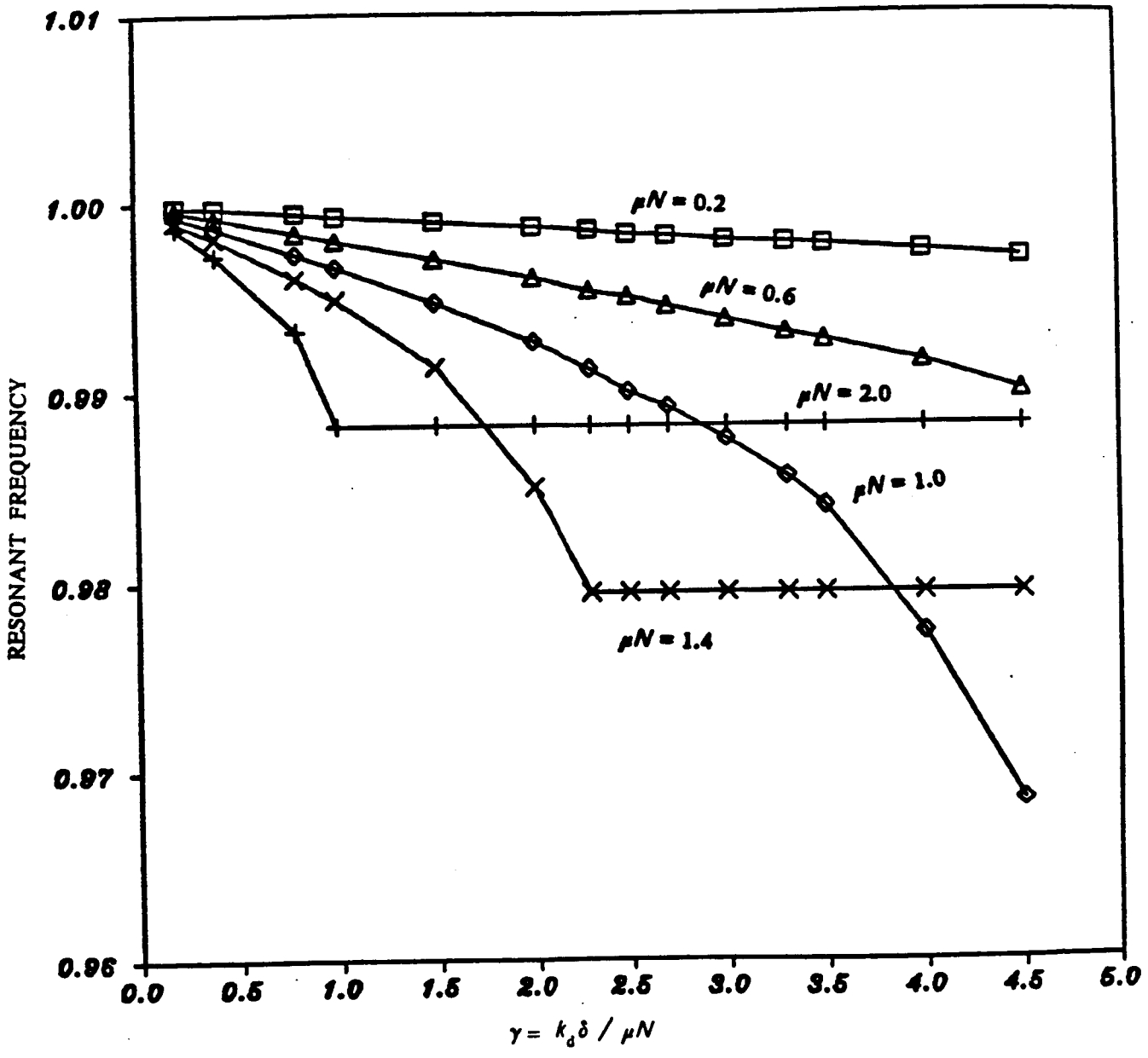

Figure 16: Resonant Frequency vs. γ, $q = 0.5$

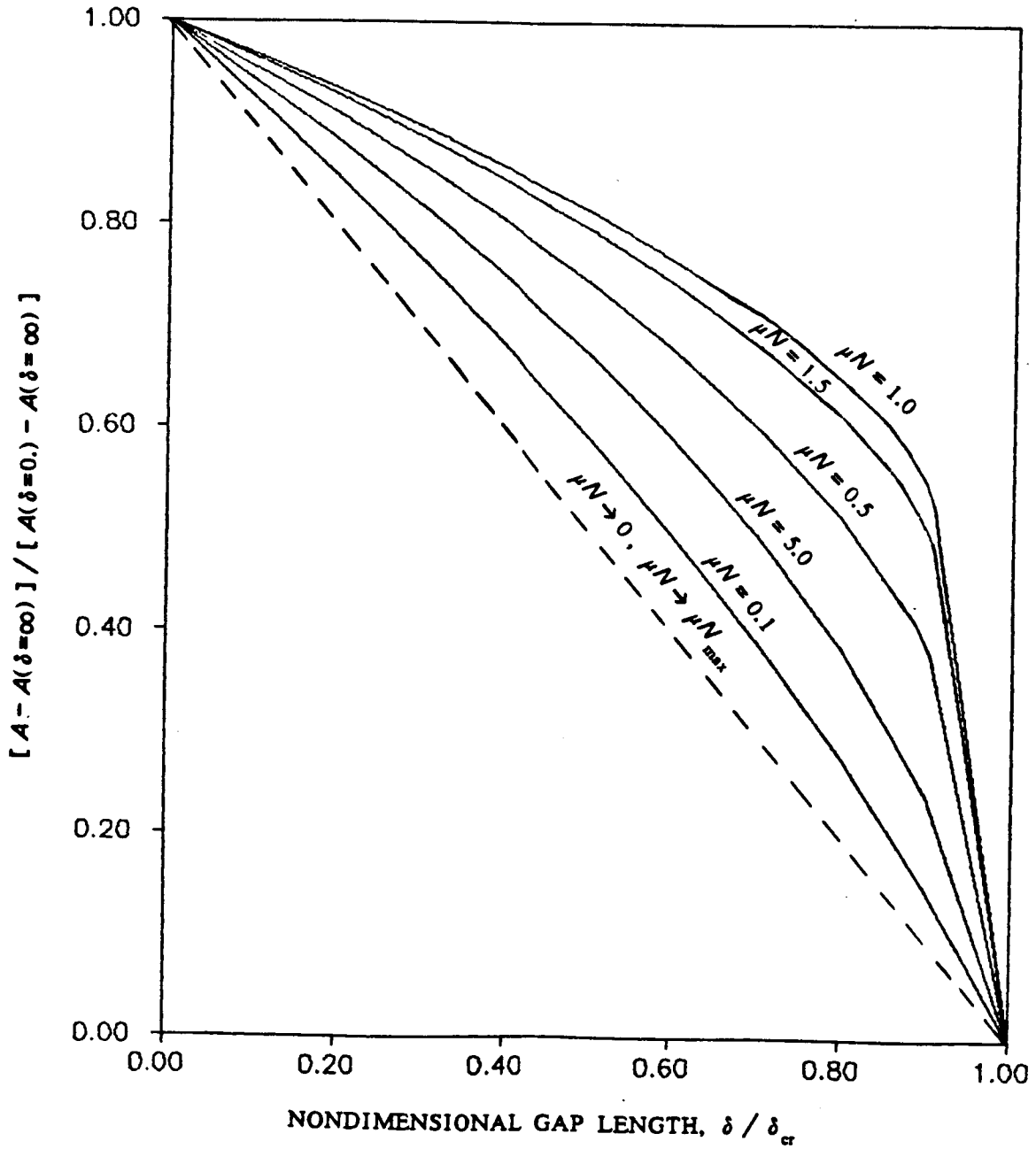

Figure 17: Scaled Max. Amplitude vs. δ/δ_{cr} with Varied Normal Load μN, $q = 0.5$

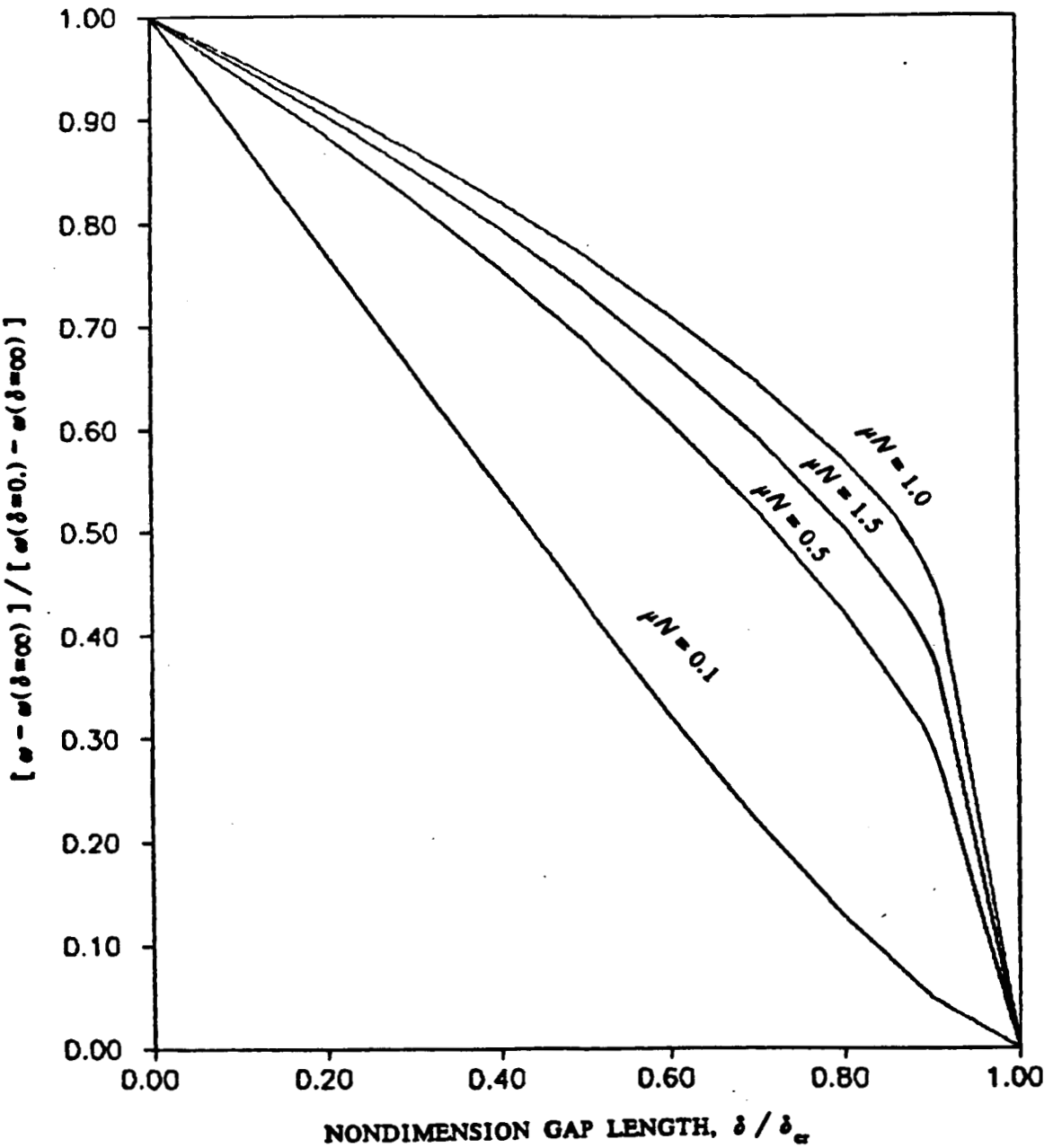

Figure 18: Scaled Resonant Frequency vs. δ/δ_{cr} with Varied Normal Load μN, $q = 0.5$

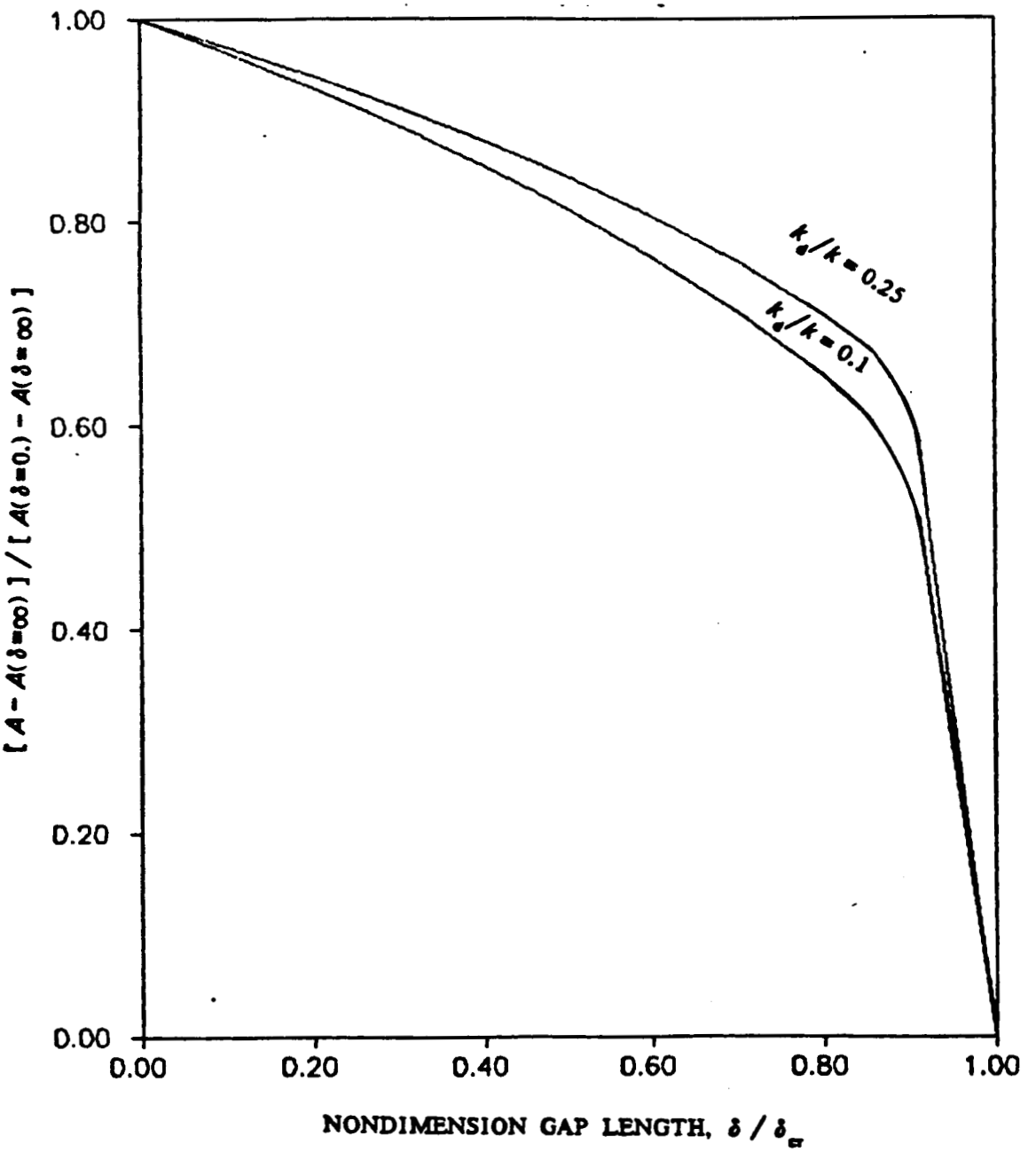

Figure 19: Scaled Max Amplitude vs. δ/δ_{cr} with Varied Stiffness k_d/k, $q = 0.5$

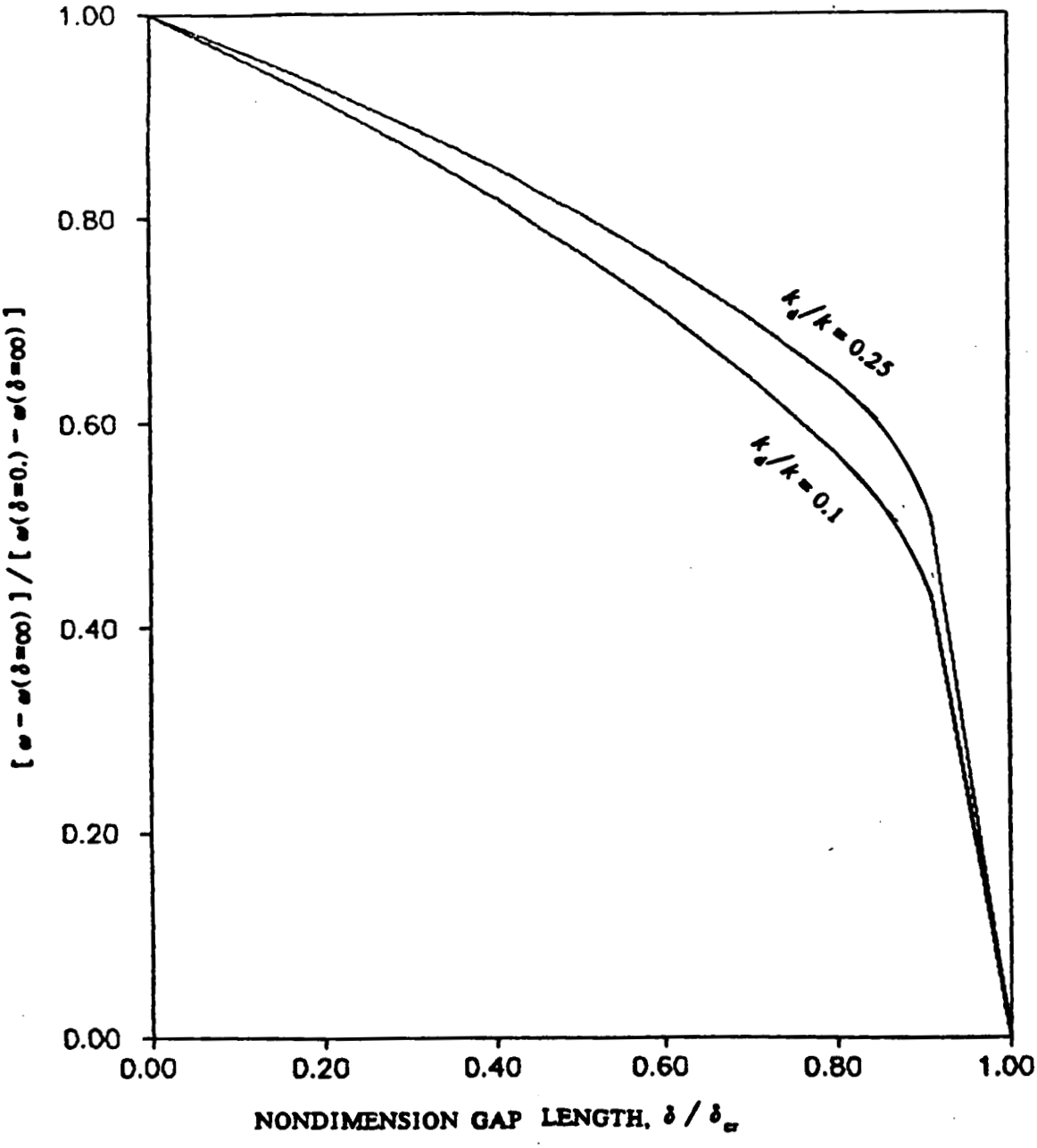

Figure 20: Scaled Resonant Frequency vs. δ/δ_{cr} with Varied Stiffness k_d/k, $q = 0.5$

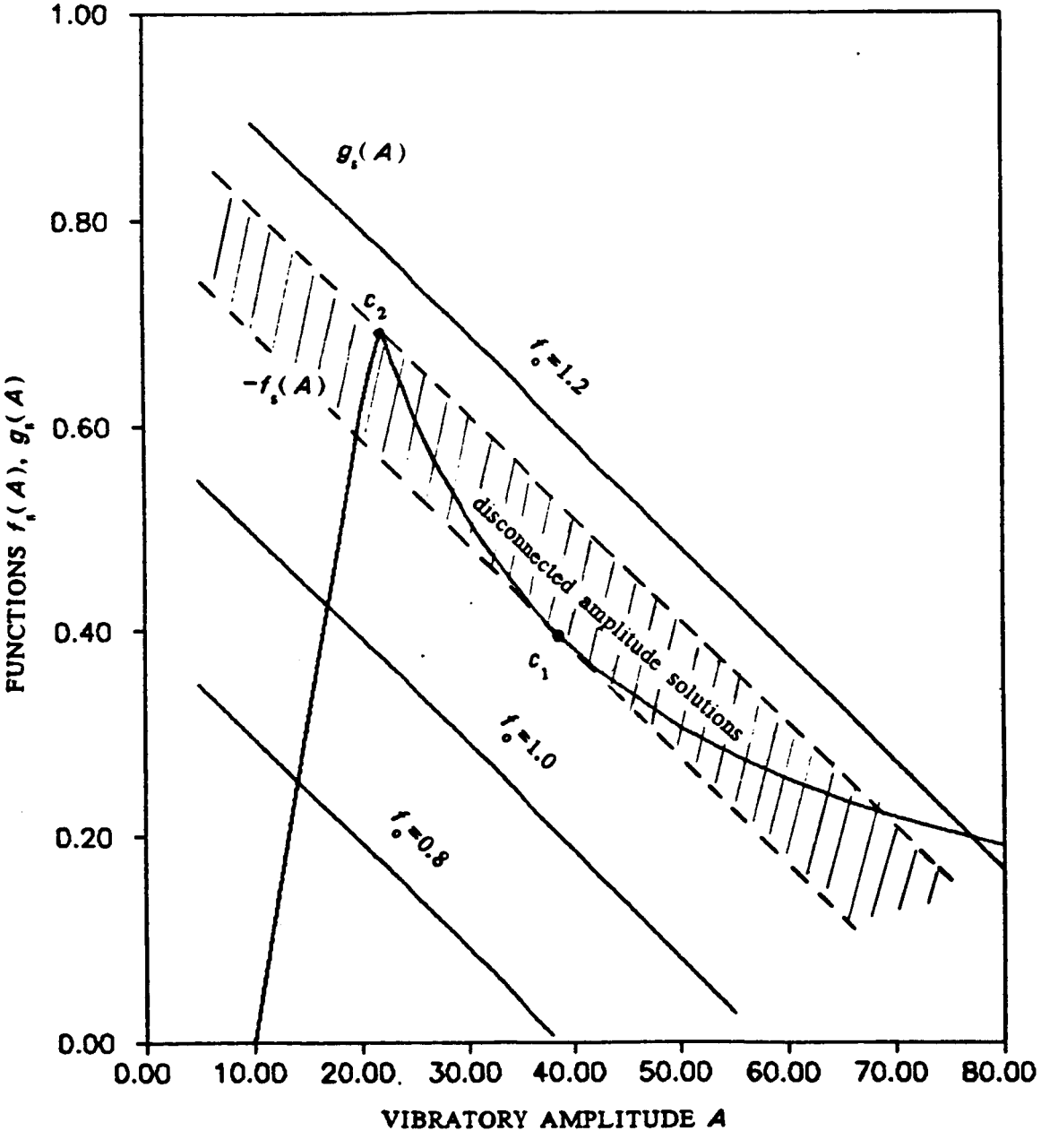

Figure 21: The Resonant Vibratory Amplitudes as is affected by the Varied Excitation f_o at constant Gap, δ=20, f_1=0, k=1.0, m=1.0, k_d=0.1, c = 0.01, μN=1.2, q=0.5

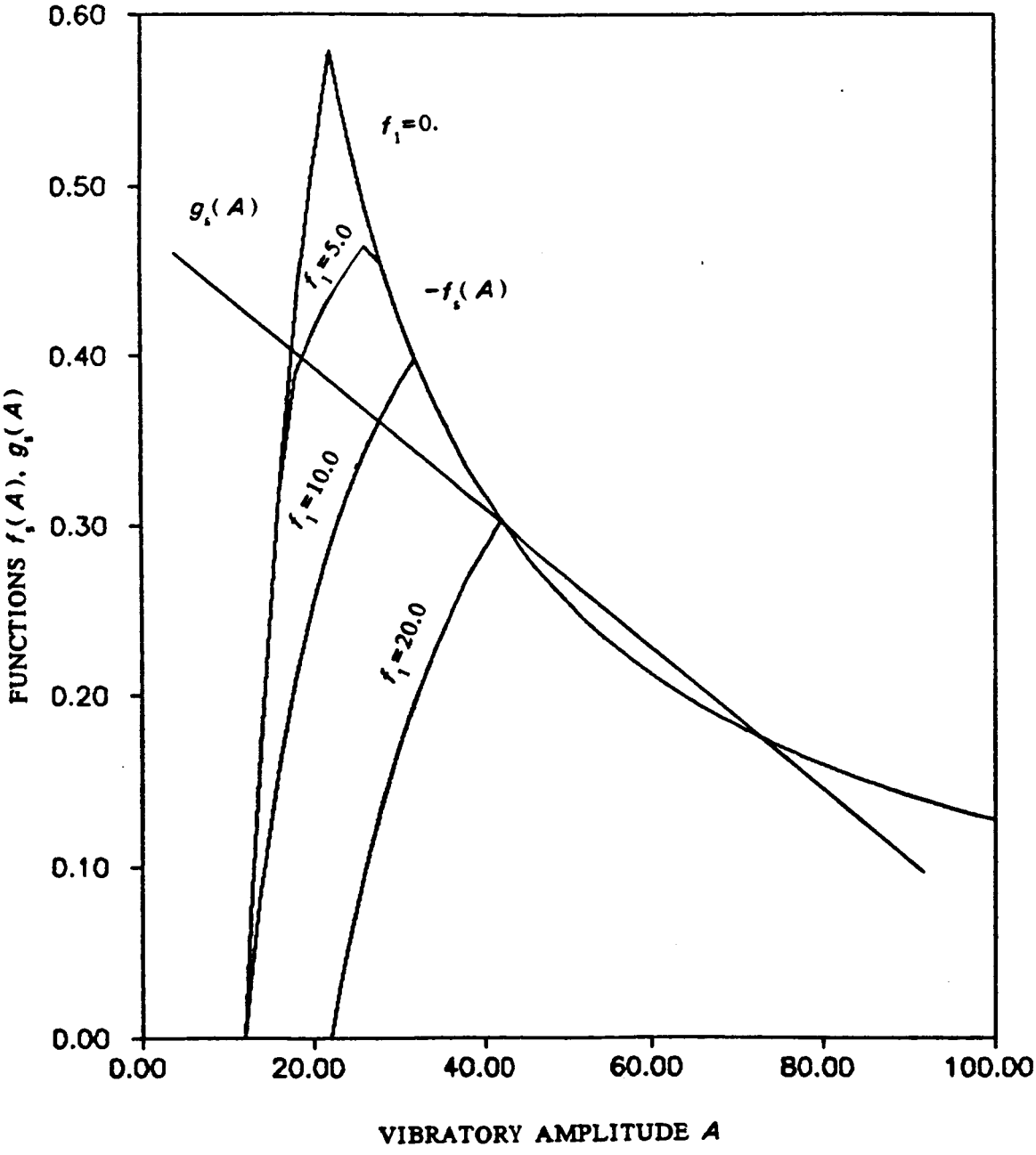

Figure 22: The Effect of Static Preload f_1 on the Resonant Amplitude Response, f_o=1.0, m = 1.0, k = 1.0, k_d=0.1, c = 0.01, μN=1.2, δ = 20, q = 0.5

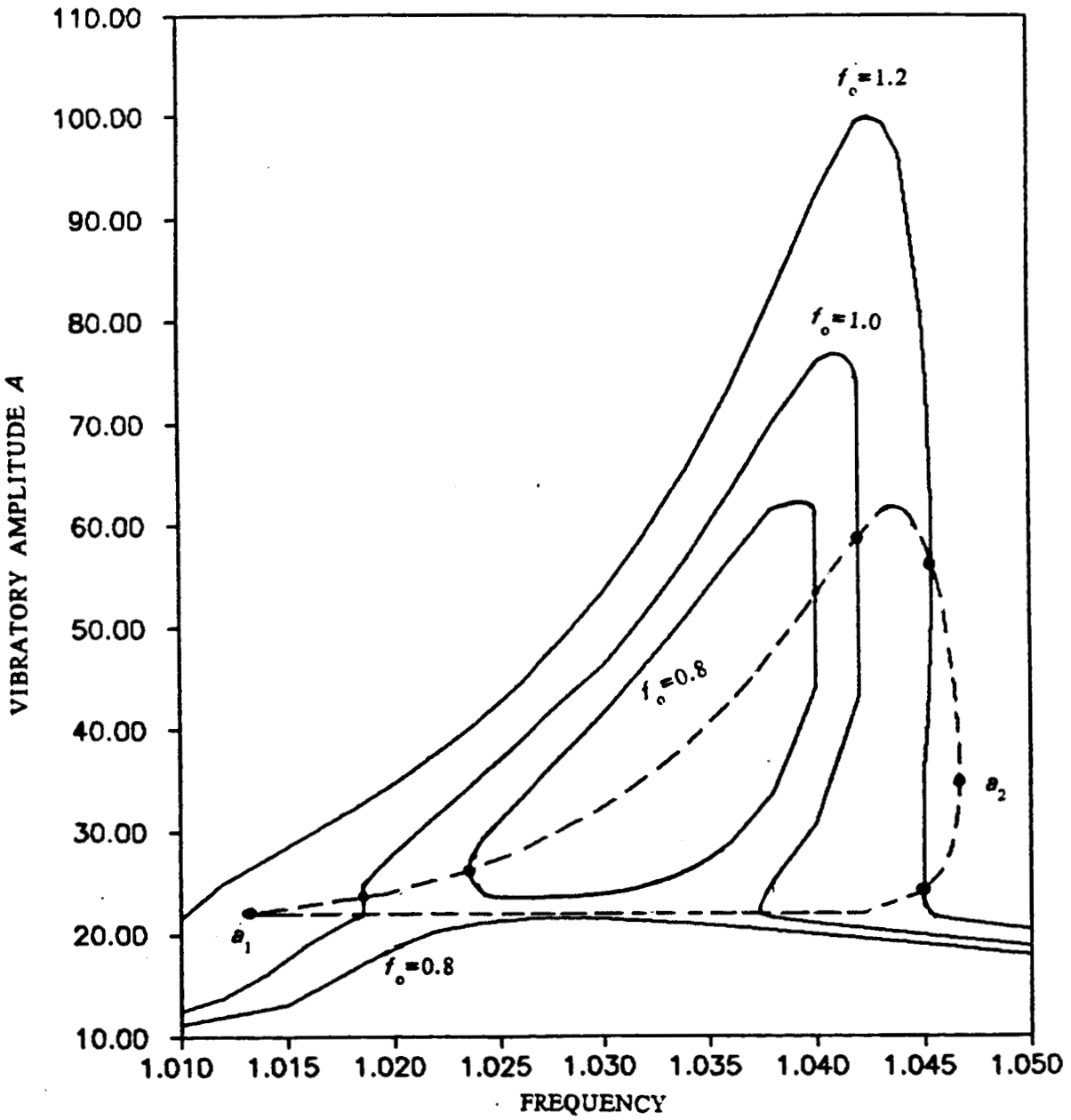

Figure 23: The Locus of Vertical Jumps in the Frequency Domain, $m = 1$, f_1=0, $k = 1.0$, k_d=0.1, c=0.01, μN=1.2, δ=20, q=0.5

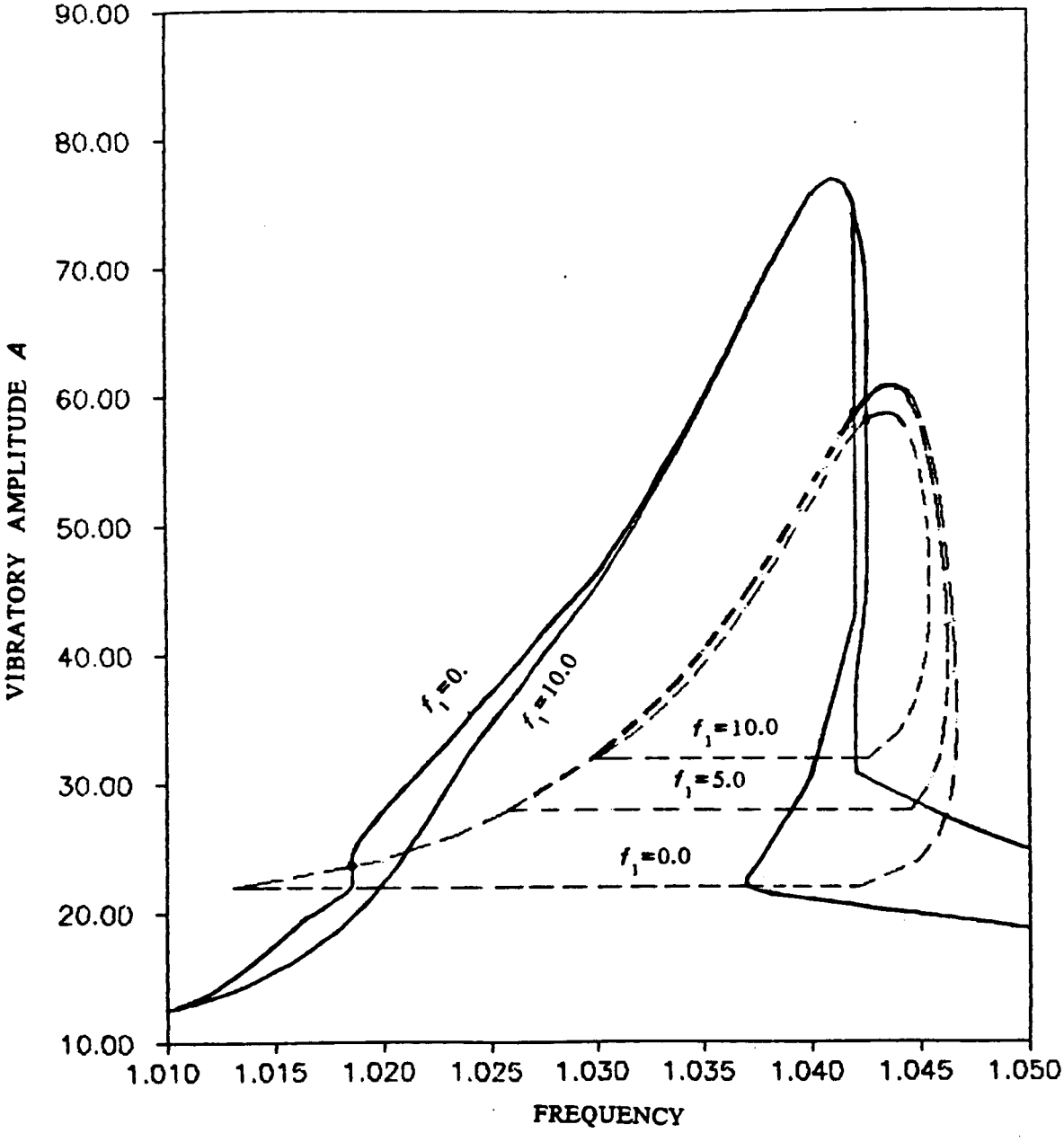

Figure 24: The Locus of Vertical Jumps as affected by the Static Load, f_o=1.0, k=1.0, m=1.0, k_d=0.1, c=0.01, δ=20, μN=1.2, q=0.5

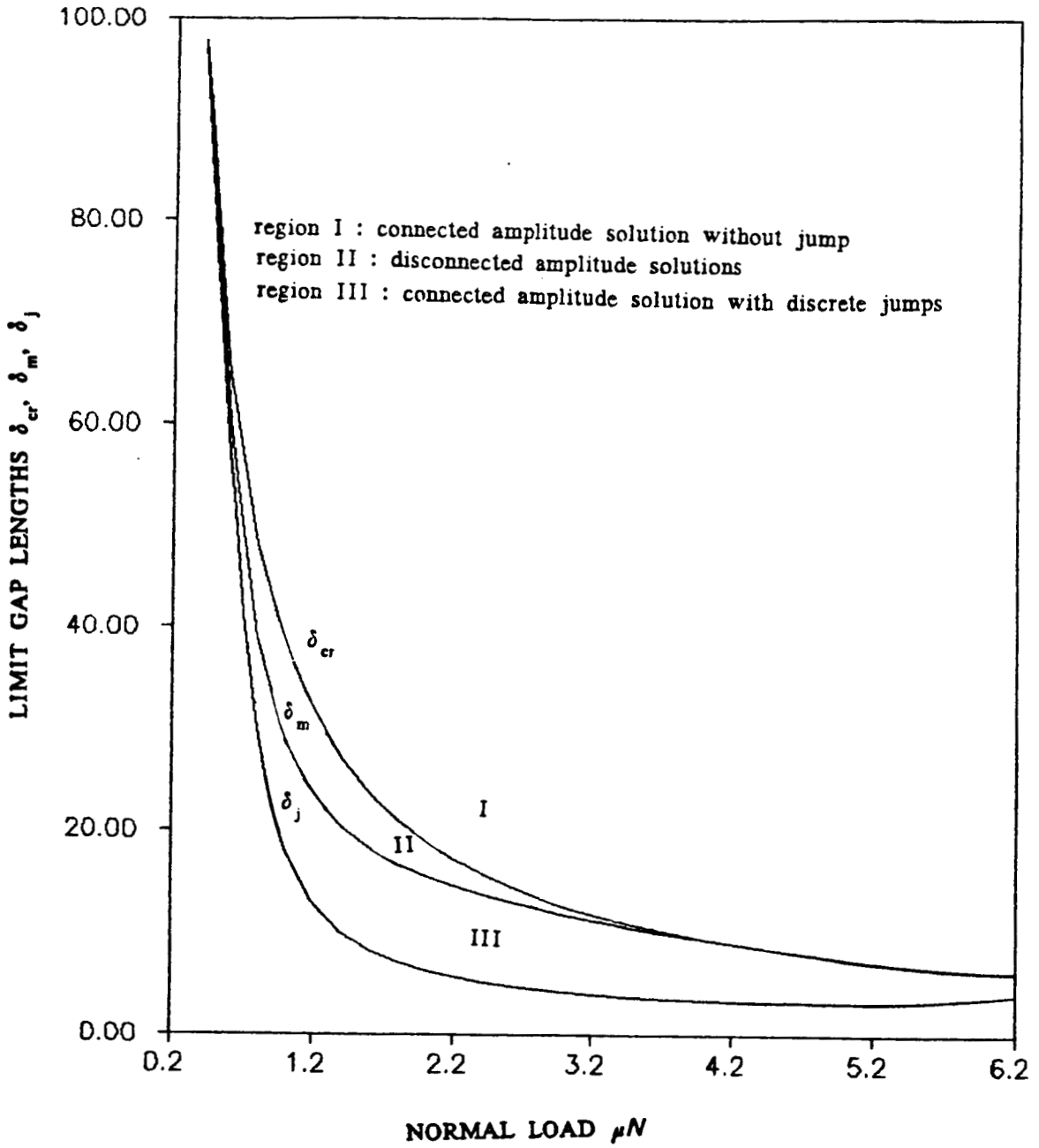

Figure 25: The Limit Gap Curves as affected by the Normal Load μN, f_o=1.0, f_j=0, k=1.0, m=1.0, k_d=0.1, c=0.01, δ=20, q=0.5

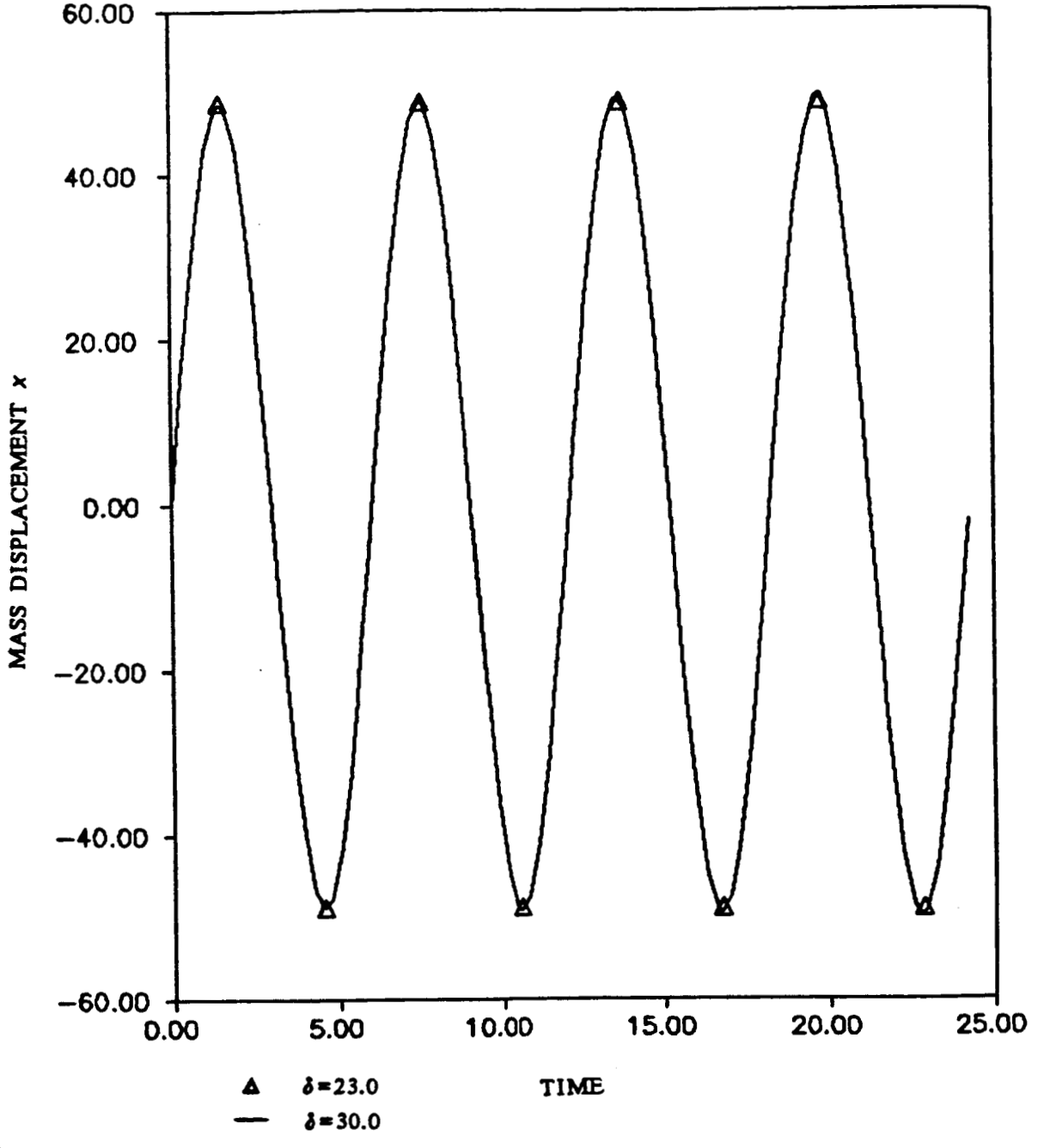

Figure 26: Effect of the Gap Length on the Transient Response [I] : Displacement vs. Time, initial pos. = 0 , initial vel. = 50, excited at ω=1.04
f_o=1.0, f_1=0 , k=1.0, m=1.0, k_d=0.1, c=0.01, μN=1.2, q=0.5

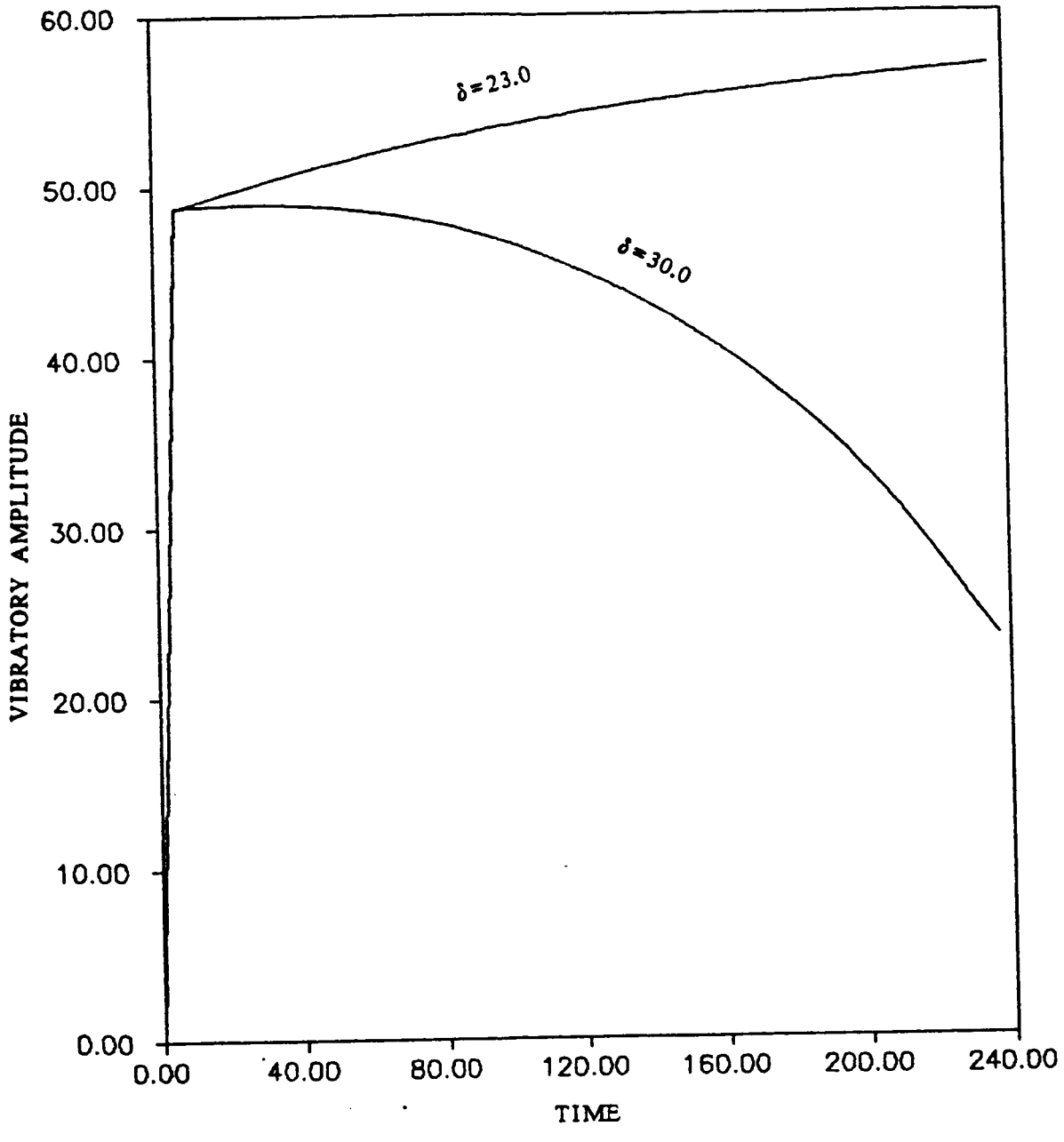

Figure 27: Effect of the Gap Length on the Transient Response [II] : Amplitude decay initial pos. =0, initial vel. = 50, excited at ω=1.04

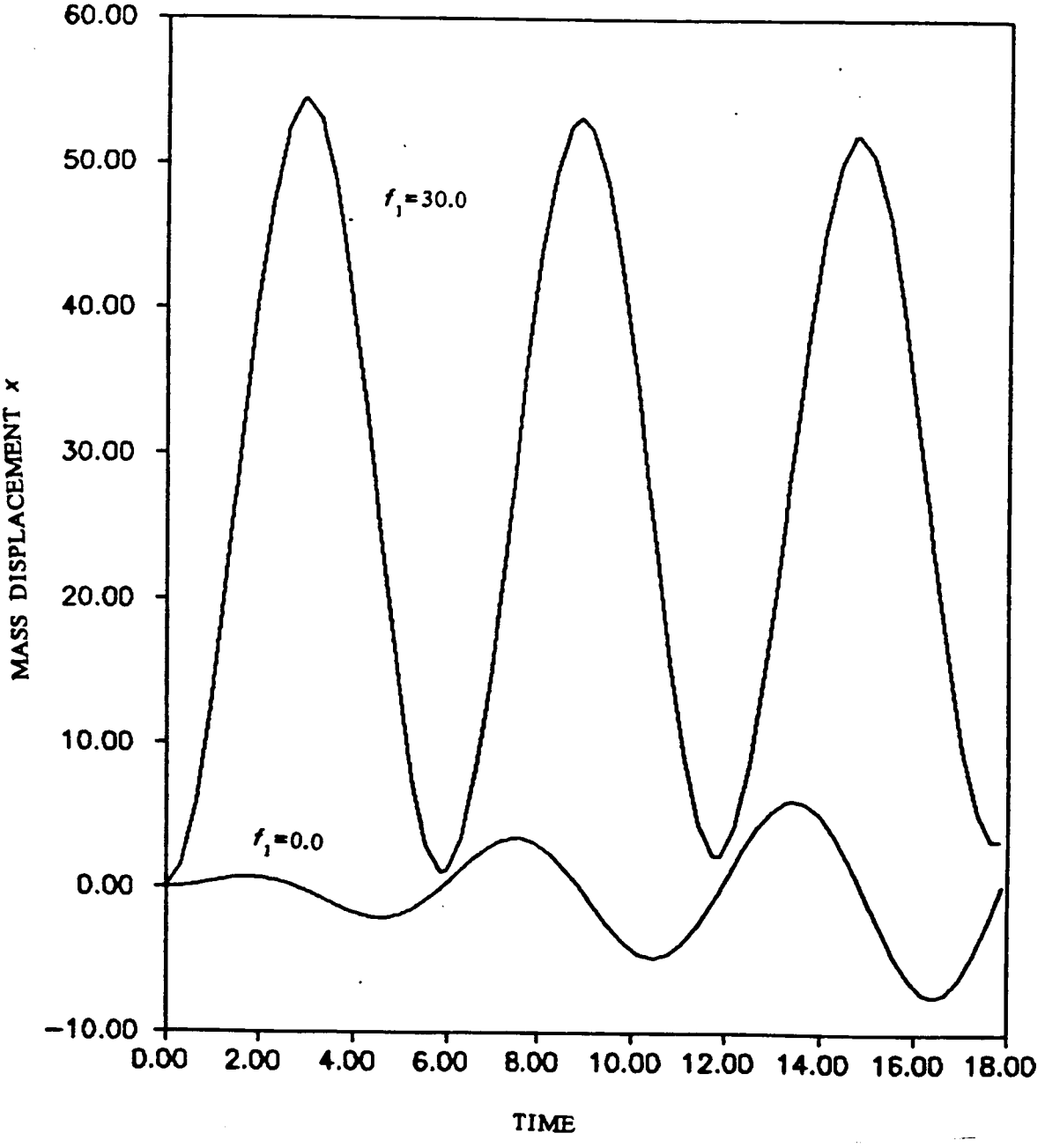

Figure 28: Effect of the Static Load f_1 on the transient response [I] : Displacement vs. Time, initial pos. = 0, initial vel. = 0, excited at ω=1.06, f_o=1.0, m=1.0, k=1.0, k_d=0.1, c=0.01, μN=2.5, δ=6.0, q=0.5

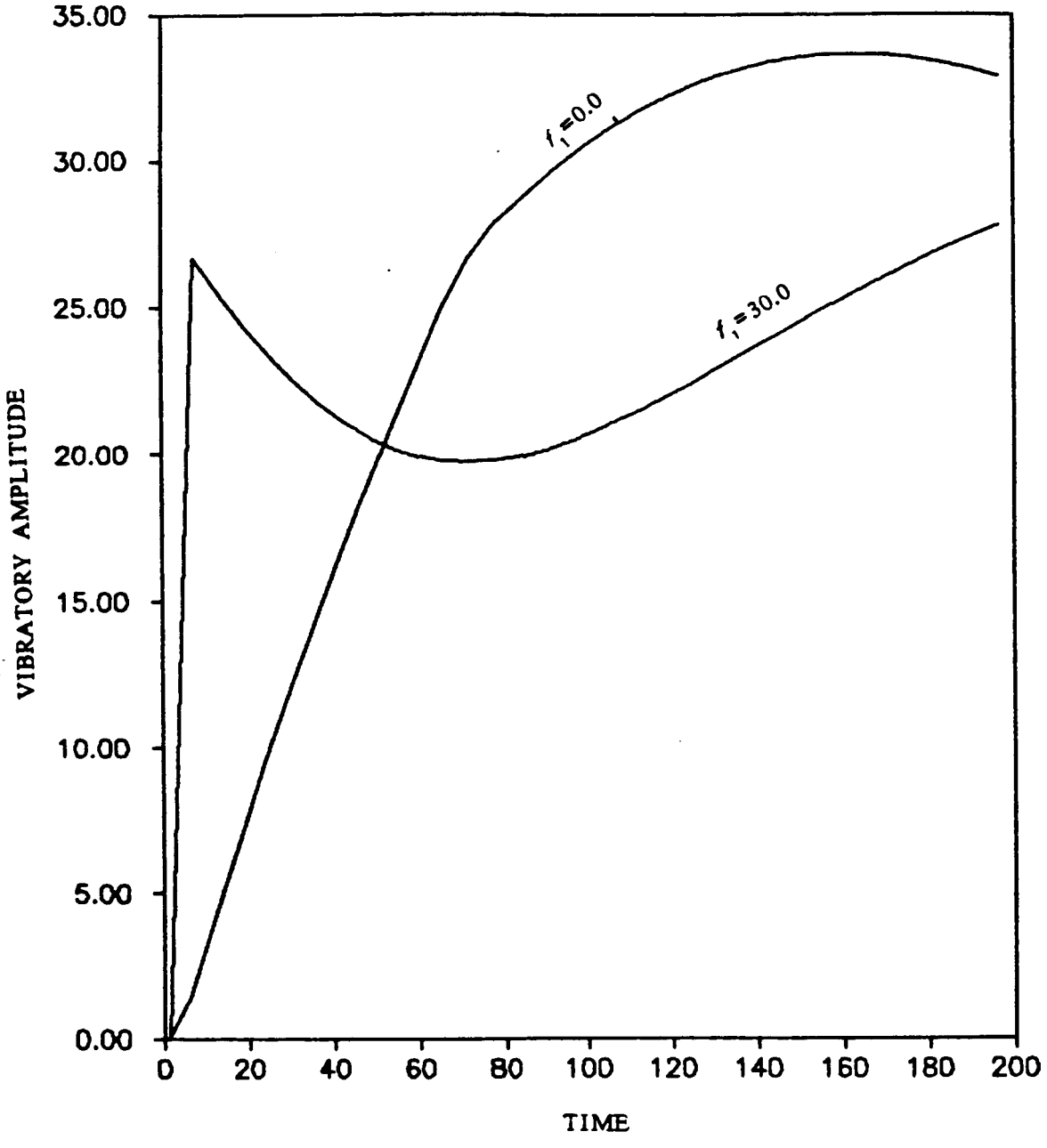

Figure 29: Effect of the Static Load f_1 on the trasient response [II] : Amplitue Decay, initial pos. = 0, initial vel. = 0, excited at ω=1.06

REFERENCES

[1] Iwan, W. D. .
Steady State Dynamic Response of a Limit Slip System.
ASME Journal of Applied Mechanics vol 35:322-326, June, 1968.

[2] Menq,C.-H. , Griffin, J. H. , and Bielak, J.
The Influence of a Variable Normal Load on the Forced Vibration of a Frictionally Damped Structure.
ASME Journal of Engineering for Gas Turbines and Power vol 108:300-305, 1986.

[3] Griffin, J. H.
Friction Damping of Resonant Stresses in Gas Turbine Engine Airfoils.
Journal of Engineering For Power vol 102(2):329-333, April, 1980.

I. APPENDIX : Calculation of Fourier Coefficient of Nonlinear Force f_n

The variations of the nonlinear friction force f_n is considered as follows:

The friction contact sticks initially, and f_n varies linearly with slope k_d. When $f_n = \pm \mu N$, it starts to slide , and f_n remains constant until the displacement x achieves an extremum or the friction contact hits either one of the stops. In the latter case, f_n again varies linearly with slope k_d until x achieves an extremum. When the mass reverses direction, the contact point again sticks and the process repeats in the opposite direction..

Given this behavior, the nonlinear force can therefore be expressed as a function of the mass's displacement during a cycle of oscillation. The Fourier coefficients can then be calculated in terms of the amplitude of vibration. To do this, the displacement is assumed to be sinusoidal plus a D.C. offset, i.e. $x = A\cos\theta + B$. Based on this, five different cases can be considered. Results for these cases are summarized in the following sections.

Case 1. No slip : $0 \le A \le \frac{\mu N}{k_d}$, and $A - \frac{\mu N}{k_d} \le B \le \frac{\mu N}{k_d} - A$

For this case, an unknown slip may occur during the transient response which results in a permanent offset at steady-state. This causes an equally unknown shift in the friction force indicated by $\bar{f}$ shown in Figure 2. The D.C. offset B and the mean value of f_n given by the Fourier coefficient f_b are related by $f_b = k_d B - \bar{f}$. While they are not known explicitly (their values depend on unknown initial conditions), they are limited in range, i.e.

$$k_d A - \mu N \le f_b \le \mu N - k_d A \tag{27}$$

In addition, the nonlinear element acts as a spring, i.e. if $f_n = f_b + f_c\cos\theta + f_s\sin\theta$ then

$$f_c = k_d A$$
$$f_s = 0$$

and the nonlinear force is in phase with the displacement.

Case 2. Pure slip : $A+B \le \delta_1 + \frac{\mu N}{k_d}$, $A-B \le \delta_2 + \frac{\mu N}{k_d}$, and $A \ge \frac{\mu N}{k_d}$

This is the case when both the stop distances δ_1, δ_2 are sufficiently large that slip is not

hindered. From Figure 3, the friction force can be divided into four sections during a displacement cycle.

$$f_n = \begin{cases} (\mu N - k_d A) + k_d A\cos\theta & , 0 \le \theta < \theta_1 \\ -\mu N & , \theta_1 \le \theta < \pi \\ (k_d A - \mu N) + k_d A\cos\theta & , \pi \le \theta < \theta_2 \\ \mu N & , \theta_2 \le \theta \le 2\pi \end{cases} \tag{28}$$

Where

$$\theta_1 = \cos^{-1}\{1 - \frac{2\mu N}{k_d A}\}$$
$$\theta_2 = \pi + \theta_1 \tag{29}$$

It is observed that the D.C. offset B has no effect on the nonlinear force f_n in this case. Using equations 27 and 28, the nonlinear force f_n can be expanded in a Fourier series as

$$f_n = f_b + f_c\cos\theta + f_s\sin\theta \tag{30}$$

Where

$$f_b = 0$$
$$f_c = \frac{1}{\pi}\{(2\mu N - k_d A)\sin\theta_1 + k_d A\theta_1\} \tag{31}$$
$$f_s = -4(\frac{\mu N}{\pi})(1 - \frac{\mu N}{k_d A})$$

Case 3. Slip with upper Limit : $A+B \ge \delta_1 + \frac{\mu N}{k_d}$, $\frac{\mu N}{k_d} - \delta_1 \le A - B \le \delta_2 + \frac{\mu N}{k_d}$

In this case (Figure 4), the upper stop is hit during the displacement cycle. Again, the nonlinear force can be separated in five sections, as shown below

$$f_n = \begin{cases} k_d(B - \delta_1) + k_d A\cos\theta & , 0 \le \theta < \theta_1 \\ -\mu N & , \theta_1 \le \theta < \pi \\ (k_d A - \mu N) + k_d A\cos\theta & , \pi \le \theta < \theta_2 \\ \mu N & , \theta_2 \le \theta < \theta_3 \\ k_d(B - \delta_1) + k_d A\cos\theta & , \theta_3 \le \theta \le 2\pi \end{cases} \tag{32}$$

Where

$$\theta_1 = \cos^{-1}\{\frac{k_d(\delta_1 - B) - \mu N}{k_d A}\}$$
$$\theta_2 = 2\pi - \cos^{-1}\{\frac{2\mu N}{k_d A} - 1\} \quad (33)$$
$$\theta_3 = 2\pi - \cos^{-1}\{\frac{k_d(\delta_1 - B) + \mu N}{k_d A}\}$$

The Fourier coefficients can be derived from equations 32 , 33 as

$$f_b = \frac{1}{2\pi}\{k_d(B - \delta_1)(2\pi + \theta_1 - \theta_3) + \mu N(\theta_1 + \theta_3 - 2\theta_2) + k_d A(\sin\theta_1 + \sin\theta_2 - \sin\theta_3 + \theta_2 - \pi)\}$$

$$f_c = \frac{1}{2\pi}\{k_d(B - \delta_1)(\sin\theta_1 - \sin\theta_3) + k_d A(\pi + \theta_1 + \theta_2 - \theta_3 + \sin\theta_2) + \mu N(\sin\theta_1 + \sin\theta_3 - 2\sin\theta_2)\} \quad (34)$$

$$f_s = -2(\frac{\mu N}{\pi})\{\frac{\delta_1 - B}{A} + 1 - \frac{\mu N}{k_d A}\}$$

Case 4. Slip with Lower Limit : $\frac{\mu N}{k_d} - \delta_2 \le A + B \le \delta_1 + \frac{\mu N}{k_d}$, $A - B \ge \delta_2 + \frac{\mu N}{k_d}$

In this case, the lower stop is hit during the displacement cycle (Figure 5). As before, the nonlinear force f_n can be separated into four sections.

$$f_n = \begin{cases} (\mu N - k_d A) + k_d A\cos\theta & , 0 \le \theta < \theta_1 \\ -\mu N & , \theta_1 \le \theta < \theta_2 \\ k_d(B + \delta_2) + k_d A\cos\theta & , \theta_2 \le \theta < \theta_3 \\ \mu N & , \theta_3 \le \theta \le 2\pi \end{cases} \quad (35)$$

Where

$$\theta_1 = \cos^{-1}\{1 - \frac{2\mu N}{k_d A}\}$$
$$\theta_2 = 2\pi - \cos^{-1}\{-\frac{\mu N + k_d(B + \delta_2)}{k_d A}\} \quad (36)$$
$$\theta_3 = 2\pi - \cos^{-1}\{\frac{\mu N - k_d(B + \delta_2)}{k_d A}\}$$

From equation 35 and 36, the Fourier coefficients are obtained.

$$f_b = \frac{1}{2\pi}\{ \mu N(2\theta_1 - \theta_2 - \theta_3 + 2\pi) + k_d A(\sin\theta_1 + \sin\theta_3 - \sin\theta_2 - \theta_1) + k_d(B + \delta_2)(\theta_3 - \theta_2)\}$$

$$f_c = \frac{1}{2\pi}\{ \mu N(2\sin\theta_1 - \sin\theta_2 - \sin\theta_3) + k_d(B + \delta_2)(\sin\theta_3 - \sin\theta_2) + k_d A (\theta_1 + \theta_3 - \theta_2 - \sin\theta_1) \} \quad (37)$$

$$f_s = -2 (\frac{\mu N}{\pi})\{ \frac{B+\delta_2}{A} - \frac{\mu N}{k_d A} + 1 \}$$

Case 5. Slip with Both Limit : $A + B \geq \delta_1 + \frac{\mu N}{k_d}$, $A - B \geq \delta_2 + \frac{\mu N}{k_d}$

In this case, both stops are hit during the displacement cycle(Figure 6). As before, the nonlinear force f_n can be divided into five sections.

$$f_n = \begin{cases} k_d(B - \delta_1) + k_d A\cos\theta & , 0 \leq \theta < \theta_1 \\ -\mu N & , \theta_1 \leq \theta < \theta_2 \\ k_d(B + \delta_1) + k_d A\cos\theta & , \theta_2 \leq \theta < \theta_3 \\ \mu N & , \theta_3 \leq \theta < \theta_4 \\ k_d(B - \delta_1) + k_d A\cos\theta & , \theta_4 \leq \theta \leq 2\pi \end{cases} \quad (38)$$

Where

$$\theta_1 = \cos^{-1}\{ \frac{k_d(\delta_1 - B) - \mu N}{k_d A}\}$$

$$\theta_2 = \cos^{-1}\{ -\frac{\mu N + k_d(B + \delta_2)}{k_d A}\}$$

$$\theta_3 = 2\pi - \cos^{-1}\{ \frac{\mu N - k_d(B + \delta_2)}{k_d A}\} \quad (39)$$

$$\theta_4 = 2\pi - \cos^{-1}\{ \frac{\mu N + k_d(\delta_1 - B)}{k_d A}\}$$

And the Fourier coefficients are derived from 38, 39 as

$$f_b = \frac{1}{2\pi}\{ k_d(B - \delta_1)(\theta_1 + 2\pi - \theta_4) + k_d(B + \delta_2)(\theta_3 - \theta_2) + k_d A(\sin\theta_1 + \sin\theta_3 - \sin\theta_2 - \sin\theta_4) + \mu N(\theta_1 + \theta_4 - \theta_2 - \theta_3)\}$$

$$f_c = \frac{1}{2\pi}\{ k_d(B - \delta_1)(\sin\theta_1 - \sin\theta_4) + k_d A(\theta_1 + \theta_3 + 2\pi - \theta_2 - \theta_4) + k_d(B + \delta_2)(\sin\theta_3 - \sin\theta_2) + \mu N(\sin\theta_1 - \sin\theta_2 + \sin\theta_4 - \sin\theta_3)\} \quad (40)$$

$$f_s = -\frac{2}{\pi}\left(\frac{\delta}{A}\right)\mu N \qquad \text{where} \qquad \delta = \delta_1 + \delta_2$$

From the above obtained results, the nonlinear force f_n can be written as

$$f_n = f_b(A, B, \mu N, k_d, \delta_1, \delta_2) + f_c(A, B, \mu N, k_d, \delta_1, \delta_2)\cos\theta + f_s(A, B, \mu N, k_d, \delta_1, \delta_2)\sin\theta \quad (41)$$

The three coefficients can be nondimensionlized as follows :

$$\begin{aligned} f_b &= \mu N F_b(\alpha, \beta, \gamma, q) \\ f_c &= \mu N F_c(\alpha, \beta, \gamma, q) \\ f_s &= \mu N F_s(\alpha, \beta, \gamma, q) \end{aligned} \quad (42)$$

where

$$\begin{aligned} \alpha &= \frac{k_d A}{\mu N} \\ \beta &= \frac{B}{\delta} \\ \gamma &= \frac{k_d \delta}{\mu N} \\ q &= \frac{\delta_1}{\delta} \end{aligned} \quad (43)$$

where, $\delta = \delta_1 + \delta_2$